CAPITAL UNIVERSITY OF SCIENCE AND TECHNOLOGY, ISLAMABAD

Sound Attenuation through Expansion Chamber having Porous Medium

by

Muhammad Tanveer

A thesis submitted in partial fulfillment for the degree of Master of Philosophy

in the

Faculty of Computing
Department of Mathematics

2021

I dedicate this effort to my dear parents, my family, my supervisor Dr. Muhammad Afzal and my elegant Teachers who are always source of inspiration for me and their contributions are uncounted.

CERTIFICATE OF APPROVAL

Sound Attenuation through Expansion Chamber having Porous Medium

by

Muhammad Tanveer

MMT183020

THESIS EXAMINING COMMITTEE

S. No.	Examiner	Name	Organization
(a)	External Examiner	Dr. Aftab Khan	COMSATS , Islamabad
(b)	Internal Examiner	Dr. Rashid Ali	CUST , Islamabad
(c)	Supervisor	Dr. Muhammad Afzal	CUST ,Islamabad

Dr. Muhammad Afzal
Thesis Supervisor
December, 2021

Dr. Muhammad Sagheer
Head
Dept. of Mathematics
December, 2021

Dr. Muhammad Abdul Qadir
Dean
Faculty of Computing
December, 2021

Author's Declaration

I, **Muhammad Tanveer** hereby state that my MPhill thesis titled "**Sound Attenuation through Expansion Chamber having Porous Medium**" is my own work and has not been submitted previously by me for taking any degree from Capital University of Science and Technology, Islamabad or anywhere else in the country/abroad.

At any time if my statement is found to be incorrect even after my graduation, the University has the right to withdraw my MPhill Degree.

Muhammad Tanveer

Registration No: MMT183020

Plagiarism Undertaking

I solemnly declare that research work presented in this thesis titled "**Sound Attenuation through Expansion Chamber having Porous Medium**" is solely my research work with no significant contribution from any other person. Small contribution/help wherever taken has been duly acknowledged and that complete thesis has been written by me.

I understand the zero tolerance policy of the HEC and Capital University of Science and Technology towards plagiarism. Therefore, I as an author of the above titled thesis declare that no portion of my thesis has been plagiarized and any material used as reference is properly referred/cited.

I undertake that if I am found guilty of any formal plagiarism in the above titled thesis even after award of MS Degree, the University reserves the right to withdraw/revoke my MS degree and that HEC and the University have the right to publish my name on the HEC/University website on which names of students are placed who submitted plagiarized work.

Muhammad Tanveer
Registration No: MMT183020

Acknowledgement

In the name of ALLAH, the most Beneficent and the most Merciful. All praises to ALLAH, Who taught (the use of) the pen, taught man that which he knew not. I bear witness that MUHAMMAD (PBUH) is the last prophet of ALLAH, Whose life is a perfect model for all mankind till the final day.

I submit my heartiest gratitude to my respected supervisor Dr. Muhammad Afzal, for his sincere guidance for completing this thesis. I am also deeply indebted to Dr. Muhammad Sagheer and other respected faculty members of Mathematics department for their invaluable help during study. I am tankful to my friends Muhammad Haroon, Adeel Arif, Farhan Ahmad and Tauqeer Nawaz who helped me alot during this work directly or indirectly. I humbly extend my thanks to all colleagues for their valuable support during research.

Finally, I sincerely thank to my parents, my brothers, my sister, my wife and other family members for their encouragement, moral support, care and prayers.

Muhammad Tanveer

Abstract

The present thesis discusses the impact of external sound source in discontinuous waveguide. The Mode-matching technique is applied to solve the governing boundary value problems. The attenuation of source radiation is analyzed through the consideration of discontinuous channel and absorbent material. The attenuation of source radiation with expansion chamber having porous medium is investigated. The truncated solution satisfies matching conditions of pressures and velocities. To insight physically, the transmission loss is investigated against frequency. It is observed that by varying the length of Chamber as well as porous medium the transmission loss is varied.

Contents

List of Figures

List of Tables

Chapter 1

Introduction

Noise pollution is the biggest problem of modern era. It not only disrupts the normal functioning of life but also affects the health of humans. The major effects of noise on humans include: physiological effects, increase of blood pressure and feeling of headache, psychological effects, stress and nervousness and social segregation. The main sources of noise are road traffic, airplanes, railways, construction sites and industrial areas. In order to reduce the unwanted noise various noise control measures are used. For example, silencers like components are employed at the exhausts of automobiles. The inside of these silencers involve various geometric designs and sound absorbing materials that minimize the vibrational waves of exhaust engines and fans.

Moreover for the noise of Heating, Ventilation and Air Conditioning (HVAC) systems of building, different duct designs and sound proofing are used. It works like a channel which transports vibrational energy from one point of the medium to another point. The investigation on designs and materials properties of such ducts in order to minimize the vibrational energy has gained much attention of researcher and engineers. The current study is relevant to the propagation and attenuation of sound radiation in a waveguide including porous material and splitting expansion chamber. The material properties of absorptive material can be varied. Such waveguides may have applications in HVAC and silencer designs.

The current study focuses on the modeling of acoustic waves, their propagation, scattering and absorption.

1.1 Background and Literature Survey

The present study is related to the propagation and scattering of acoustics waves in rectangular waveguide or channel. The performance of acoustical waveguide to reduce unwanted noise can be increased by using the noise absorbent material and/or introducing the locally reactive liners. The salient features of acoustics scattering in guiding structures that contain expansions and/or contractions in geometry have vital role in noise reduction applications. For example, expansion chambers are widely used to reduce unwanted exhaust noise produced by internal combustion engines that travels through the duct.

The propagation of wave along the ducts with rapid changes in the cross sectional area can produce reactions that reduce the energy of transmitted wave. This is the method together with cavity resonance mechanisms by which silencer box reduce noise in the car exhaust system [1]. Hassan and Rawlins [2], Rawlins [3, 4] and Ayub et al. [5–7] discussed the propagation of sound waves in cylinderical channel containing sound absorbing linings along the walls of the channel. They used Wiener Hopf technique to analyze the effects of absorbing material. Lawrie and Afzal [8] are concerned with the reflection and transmission of fluid-structure-coupled waves at the junction between two flexible waveguides of different heights. Ayub et al. [9] and Huang [10–12] considered the reactive silencer used in HVAC system for reducing ducted tonal fan noise.

Using the silencer eigenmodes in an analytic Mode-matching approach, Cummings and Chang [13] enforced pressures and velocities continuity over the inlet and outflow planes of the silencer. Cummings and Chang's method was offered by Peat [14] and afterwards by Kirby [15] as a more efficient alternative. They developed

closed form analytic solutions based solely on the fundamental mode's attenuation. Peat and Kirby's approaches, on the other hand, are accurate only across a limited frequency range for a given waveguide structure. Folk and Herczynski [16, 17] worked on the class of problems in which there are second and higher order boundary conditions at the duct wall. They utilized the idea of separation of a variable method to reduce the equation into a system of coupled and uncoupled second order ordinary differential conditions, which were solved by utilizing the boundary conditions. This outcome into a Strum-Liouville eigensystem and there is a need to determine an orthogonality relation to solve the problem.

A Mode-matching method was used [18] to evaluate the sound waves in a three-part duct containing porous material attached to the wall. Lawrie and Kirby [19] use the Mode-matching technique for the analysis of absorbent silencer. In general there are two possible approaches to modelling finite length (bulk reacting) dissipative silencers, one may analyse the problem numerically, which generally involves the use either of the finite element method [20] or the boundary element method [21], alternatively one may approach the problem analytically, which typically involves finding roots of the governing dispersion relation and using orthogonality relation to match the acoustic pressure and velocity fields over the inlet and outlet planes of the silencer. Sound attenuation in rigid-walled ducts with bulk-reacting, sound-absorbent porous liners or splitters has been fairly extensively studied, both in the absence and in the presence of mean gas flow see refrances [22–27].

Cummings [28] discussed the attenuation of sound in ducts lined on two opposite walls with porous material with some applications to splitter. Astley and Cummings [29] used finite element scheme for attenuation in duct lined with porous material. Lawrie and Kirby [30] discussed a point collocation approach to modelling large dissipative silencers. The wave scatters through flexible guiding channels together with structural variations is discussed in [31–47]. Accordingly, the dispersion of waves through different layered medium is discussed in [48–66]. The present work is in continuation of the aforementioned studies with expansion chamber containing sound absorbent material along with backward propagation. The

influence of wall motion on sound propagation in unlined rectangular ducts with flexible walls has been examined [70] in a study of noise break-out duct-work, and it has also been shown [71] that structural/acoustic wave combinations exist wherein the energy flow can concentrate itself predominantly either in the structure or in the fluid contained in the duct. In this thesis propagation of sound source is investigated by using mode-matching technique and transmission loss is calculated.

1.2 Thesis Structure

The rest of the thesis is organized as follows.

Chapter 1 The chapter wise details of the present study are enclosed in this chapter. This chapter depicts background and literature survey relevant to the current study along with thesis structure.

Chapter 2 comprises some basic definitions, physical laws, formulation of wave equation and useful derivations.

Chapter 3 contains the propagation of acoustic waves in discontinuous waveguide. Also this chapter includes sound absorbent material.

Chapter 4 includes four regions and second region involves porous material.

chapter 5 provides the summary and concluding remarks of the thesis.

References used in the thesis are mentioned in **Bibliography**

Chapter 2

Preliminaries

This thesis contains physical problems that are relevant to the reflection, transmission and absorption of acoustic waves propagating in rectangular ducts or channels. The purpose of present chapter is to discuss some basic terminologies which are useful in understanding the mathematical modeling and associated physical characteristics of the work presented in rest of the chapters.

2.1 Acoustics

Acoustics is the branch of science which deals with the propagation of mechanical waves in matter. This branch covers how sound energy emits, reflect and transmits through a medium. The word acoustics is derived from a Greek letter akoustikos which means to hear. Normal human frequency range of hearing lies between 20Hz to 20K.Hz. The vibrations with frequency less than 20Hz is known as infra sound and above than 20K.Hz is ultra sound.

2.2 Wave

Wave is the disturbance in the medium which causes the particles of that medium to vibrate from one place to another to transfer the energy. It is important to know

that waves transfer energy of the matter without transferring matter. Typical examples include light waves and sound waves etc.

2.2.1 Types of Wave

There are three types of waves based on the medium characteristics and energy propagation. These types include:

Mechanical waves

The type of wave in which energy is transfered through the oscillation produced in a material medium. Examples include waves produce on the strings, springs and on water surface.

Longitudinal wave

The waves in which direction of particles of medium are parallel to the direction of propagation of waves. Examples are, sound and pressure waves.

Transverse waves

The waves in which the direction of particles is perpendicular to the direction of propagation waves.

Electromagnetic waves

The waves which are produced when electric and magnetic fields oscillate perpendicular to each other. These waves do not need any material medium for transfer of energy. Examples include radio waves, microwaves and X-rays.

2.3 Acoustic Wave Equation

The wave propagation in a medium can be expressed in terms of wave equation which can be derived by using conservation of mass, momentum and equation of state. The derivation of wave equation can be found in [67],

$$\nabla^2\Phi = \frac{1}{c^2}\frac{\partial^2\Phi}{\partial t^2}, \tag{2.1}$$

where c is the speed of sound in compressible fluid.

2.4 Acoustic Monopoles Source

An acoustic monopole radiates sound equally in all directions. An example of an acoustic monopole would be a small sphere whose radius alternately expands and contracts. In practice, any sound source whose dimensions are much smaller than the wavelength of the sound being radiated will act as a monopole, radiating sound equally well in all directions. The sound pressure of a monopole source can be expressed as follows

$$\mathbf{p}(r) = \mathbf{S}\ \frac{e^{jkr}}{r}, \tag{2.2}$$

where the complex variable $\mathbf{S}$ is the monopole amplitude. Here, the amplitude of the sound source is the inertial force of fluid mass that the sound source exerts per unit time and unit solid angle. In other words, it can be expressed as

$$\mathbf{S} = \frac{1}{4\pi}\rho_0(-j\omega\mathbf{q}), \tag{2.3}$$

where $\mathbf{q}$ represents the volume velocity which is radiated by a monopole sound source per unit time.

From Euler's equation, the velocity for the r direction can be written as

$$\mathbf{U}_r(r) = \frac{1}{jk\rho_0 c}\frac{\partial \mathbf{p}}{\partial r} = \frac{\mathbf{S}e^{jkr}}{\rho_0 cr}\left[1 + j(\frac{1}{kr})\right]. \tag{2.4}$$

The velocity in near-field and far-field sound fields are approximately obtained as

Near field ($kr << 1$):

$$\mathbf{U}_r(r) \approx \frac{\mathbf{S}e^{jkr}}{\rho_0 cr} j(\frac{1}{kr}). \tag{2.5}$$

Far field ($kr >> 1$):

$$\mathbf{U}_r(r) \approx \frac{\mathbf{S}e^{jkr}}{\rho_0 cr}. \tag{2.6}$$

From (2.2) and (2.4), the impedance can also be obtained as

$$\mathbf{Z}_r(r) = \frac{\mathbf{p}(r)}{\mathbf{U}_r(r)} = \rho_0 c \frac{1}{1 + j(\frac{1}{kr})}. \tag{2.7}$$

Near- field:

$$\mathbf{Z}_r(r) \approx -j\rho_0 c(kr). \tag{2.8}$$

Far-field:

$$\mathbf{Z}_r(r) \approx \rho_0 c. \tag{2.9}$$

Equation (2.9) implies that it becomes a plane wave in a far field.

2.5 Boundary Conditions

The following boundary conditions are defined to model the BVP:

1. Soft conditions.

2. Rigid conditions.

3. Impedance conditions.

2.5.1 Soft Conditions

The soft boundary conditions are Drichlet's type boundary conditions. In these conditions, the pressure or displacement is taken as zero, i.e.

$$\Phi(x, y) = 0.$$

2.5.2 Rigid Conditions

Neumann's type boundary conditions are actually rigid boundary conditions. In rigid conditions, normal velocity is taken as zero, i.e.

$$\frac{\partial \Phi}{\partial x} = 0.$$

2.5.3 Impedance Conditions

The impedance boundary conditions are Robin's type boundary conditions. Robin boundary conditions are combination of Drichlet boundary conditions and Neumann boundary conditions. These conditions are written as

$$\beta_1 \Phi(x, y) + \beta_2 \frac{\partial \Phi(x, y)}{\partial x} = 0,$$

where β_1 and β_2 are arbitrary constants.

2.6 Delta Function

When working with sound sources, delta function is crucial. The delta function $\delta(p - p')$ is defined as

$$\delta(p - p') = 0, \quad p \neq p', \tag{2.10}$$

$$\delta(p - p') = \infty, \quad p = p', \tag{2.11}$$

and

$$\int_V \delta(p - p') dv = 1 \quad \text{when volume V contains } \ p'. \tag{2.12}$$

The shifting property of delta function is

$$\int_V f(p)\delta(p-p')dv = f(p'). \tag{2.13}$$

Take into account the delta function $\delta(p-p')$ where $x = x'$ is the location of the source. Then

$$\delta(p-p') = \delta(x-x'). \tag{2.14}$$

Likewise, for two-dimensional rectangular coordinates, we can write

$$\delta(p-p') = \delta(x-x')\delta(y-y'). \tag{2.15}$$

2.7 Sturm-Liouville Equation

Assume differential equation

$$\left\{\frac{d}{dx}\left[f(x)\frac{d}{dx}\right] + g(x) + \lambda_n h(x)\right\}\varphi_n(x) = 0. \tag{2.16}$$

In between $a_1 \leq x \leq b_1$ subject to restrictions

$$\left[\alpha_1\varphi_n(x) + \beta_1\frac{d\varphi_n(x)}{dx}\right]_{x=a_1} = 0, \tag{2.17}$$

$$\left[\alpha_2\varphi_n(x) + \beta_2\frac{d\varphi_n(x)}{dx}\right]_{x=b_1} = 0, \tag{2.18}$$

note that the functions $f(x)$, $g(x)$ and $h(x)$ including the parameters α_1, α_2, β_1 and β_2 seem to be real.

When $f(x) = 1$, $g(x) = 0$, $\lambda_n = k_n^2$ and $h(x) = 1$, (2.16) turns into simple harmonic motion differential equation.i.e

$$\left\{\frac{d^2}{dx^2} + k_n^2\right\}\varphi_n(x) = 0. \tag{2.19}$$

Let's demonstrate that the eigenfunctions are orthogonal. Multiplying (2.16) by $\varphi_m^*(x)$, where $*$ denotes complex conjugate and integrate from a_1 to b_1 gives

$$\int_{a_1}^{b_1} \varphi_m^*(x) \frac{d}{dx}\left[f(x)\frac{d\varphi_n(x)}{dx}\right] dx + \int_{a_1}^{b_1} g(x)\varphi_m^*(x)\varphi_n(x)dx + \lambda_n \int_{a_1}^{b_1} h(x)\varphi_m^*(x)\varphi_n(x)dx = 0. \tag{2.20}$$

Integration by parts gives

$$\begin{aligned}
&\int_{a_1}^{b_1} \varphi_m^*(x) \frac{d}{dx}\left[f(x)\frac{d\varphi_n(x)}{dx}\right] dx \\
&= \left[\varphi_m^*(x) f(x)\frac{d\varphi_n(x)}{dx}\right]_{a_1}^{b_1} - \int_{a_1}^{b_1} \frac{d\varphi_m^*(x)}{dx} f(x)\frac{d\varphi_n(x)}{dx}dx \\
&= f(a_1)\frac{\alpha_1}{\beta_1}\varphi_m^*(a_1)\varphi_n(a_1) - f(b_1)\frac{\alpha_2}{\beta_2}\varphi_m^*(b_1)\varphi_n(b_1) - \int_{a_1}^{b_1} \frac{d\varphi_m^*(x)}{dx} f(x)\frac{d\varphi_n(x)}{dx}dx.
\end{aligned} \tag{2.21}$$

Now on invoking (2.21) into (2.20), we get

$$\begin{aligned}
&f(a_1)\frac{\alpha_1}{\beta_1}\varphi_m^*(a_1)\varphi_n(a_1) - f(b_1)\frac{\alpha_2}{\beta_2}\varphi_m^*(b_1)\varphi_n(b_1) - \int_{a_1}^{b_1} \frac{d\varphi_m^*(x)}{dx} f(x)\frac{d\varphi_n(x)}{dx}dx \\
&+ \int_{a_1}^{b_1} g(x)\varphi_m^*(x)\varphi_n(x)dx + \lambda_n \int_{a_1}^{b_1} h(x)\varphi_m^*(x)\varphi_n(x)dx = 0.
\end{aligned} \tag{2.22}$$

When the indices m, n are swapped and taking complex conjugate of (2.22), we get

$$\begin{aligned}
&f(a_1)\frac{\alpha_1}{\beta_1}\varphi_n(a_1)\varphi_m^*(a_1) - f(b_1)\frac{\alpha_2}{\beta_2}\varphi_n(b_1)\varphi_m^*(b_1) - \int_{a_1}^{b_1} \frac{d\varphi_n(x)}{dx} f(x)\frac{d\varphi_m^*(x)}{dx}dx + \\
&\int_{a_1}^{b_1} g(x)\varphi_n(x)\varphi_m^*(x)dx + \lambda_m^* \int_{a_1}^{b_1} h(x)\varphi_n(x)\varphi_m^*(x)dx = 0.
\end{aligned} \tag{2.23}$$

Subtracting (2.23) from (2.22), finally yields

$$(\lambda_n - \lambda_m^*) \int_{a_1}^{b_1} h(x)\varphi_n(x)\varphi_m^*(x)dx = 0. \tag{2.24}$$

Suppose that $h(x)$ does not change sign in between (a_1, b_1). For $m \neq n$

$$\int_{a_1}^{b_1} h(x)\varphi_n(x)\varphi_m^*(x)dx = 0. \tag{2.25}$$

For $m = n$

$$\int_{a_1}^{b_1} h(x)\varphi_n(x)\varphi_m^*(x)dx \neq 0, \tag{2.26}$$

$$\lambda_n - \lambda_n^* = 0. \tag{2.27}$$

The eigenfunctions $\varphi_n(x)$ are normalized as

$$\int_{a_1}^{b_1} h(x)\varphi_n(x)\varphi_m^*(x)dx = 1. \tag{2.28}$$

The condition $\lambda_n = \lambda_n^*$ shows that the eigenvalues are real. The property (2.25) and (2.28) referred to orthogonality of the eigenfunctions $\varphi_n(x)$. Eigenfunctions $\varphi_n(x)$ make up a whole set. This whole set means that any given function $q(x)$ can be expressed as a linear combination $\varphi_n(x)$ to any desired accuracy.

$$q(x) = \sum_{n=0}^{\infty} q_n\varphi_n(x). \tag{2.29}$$

On multiplying (2.29) by $h(x)\varphi_m^*(x)$ and integrating over a_1 to b_1, gives the expansion coefficient

$$q_n = \int_{a_1}^{b_1} h(x)q(x)\varphi_n^*(x)dx. \tag{2.30}$$

2.8 Definition of Fourier Transform

If $\Phi(x)$ is a continuous, piecewise smooth, absolutely integrable function, then the Fourier transform of $\Phi(x)$ is

$$F\{\Phi(x)\} = \tilde{\Phi}(\alpha) = \frac{1}{\sqrt{2\pi}} \int_{-\infty}^{\infty} e^{-i\alpha x}\Phi(x)dx, \tag{2.31}$$

where α is Fourier transform variable. The inverse Fourier transform of $\tilde{\Phi}(\alpha)$ can be defined as

$$F^{-1}\{\tilde{\Phi}(\alpha)\} = \Phi(x) = \frac{1}{\sqrt{2\pi}} \int_{-\infty}^{\infty} e^{i\alpha x} \tilde{\Phi}(\alpha) d\alpha. \tag{2.32}$$

Fourier transform of n^{th} derivative

Let Φ be continuous and piecewise smooth over $(-\infty, \infty)$ and $\Phi(x)$ approach zero as $|x| \to \infty$. If Φ and Φ^n are absolutely integrable, then

$$F\left[\Phi^n(x)\right] = (i\alpha)^n F\left[\Phi(x)\right] = (i\alpha)^n \tilde{\Phi}(\alpha), \quad n = 0, 1, 2... \tag{2.33}$$

2.8.1 One-Dimensional Green's Function

In this section, we discuss the derivation of one-dimensional Green's function in free space. The derivation is useful in chapters 3 and 4.
In one-dimensional free space $(-\infty < x < \infty)$, consider Sturm-Liouville equation with the parameters $f(x) = h(x) = 1, g(x) = 0$ and $\lambda = k^2$, which may be written as

$$\left\{\frac{d^2}{dx^2} + k^2\right\} \Phi(x, x') = -\delta(x - x'), \tag{2.34}$$

under the presence of the radiation condition $\Phi(\pm\infty; x') = 0$. The response $\Phi(x, x')$ at x is due to the delta source at x', as shown in Fig.1.

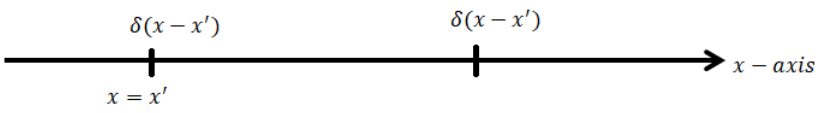

FIGURE 2.1: Free space Green's function

In terms of eigenfunctions, $\Phi(x;x')$ can be represented in inverse Fourier transform

$$\Phi(x,x') = \frac{1}{2\pi}\int_{-\infty}^{\infty} \tilde{\Phi}(\alpha;x')e^{i\alpha}d\alpha. \tag{2.35}$$

On invoking (2.35) as well as the identity

$$\delta(x-x') = \frac{1}{2\pi}\int_{-\infty}^{\infty} e^{i\alpha(x-x')}d\alpha,$$

into (2.34) yields

$$\Phi(x,x') = \int_{-\infty}^{\infty} \frac{1}{2\pi}\frac{e^{i\alpha(x-x')}}{\alpha^2-k^2}d\alpha. \tag{2.36}$$

The physical condition requires that the delta source response $\Phi(x,x')$ be an outgoing wave in the form of e^{ikx} that vanishes as $x \longrightarrow \infty$. If the medium is supposed to be slightly lossy, this condition can be met, where the medium wavenumber $k = k_r + ik_i$ has an infinitesimally small positive imaginary part ($k_i > 0$). For $x - x' > 0$, let us use the residue theorem in the complex $\alpha - plane$, as shown in Fig.2.

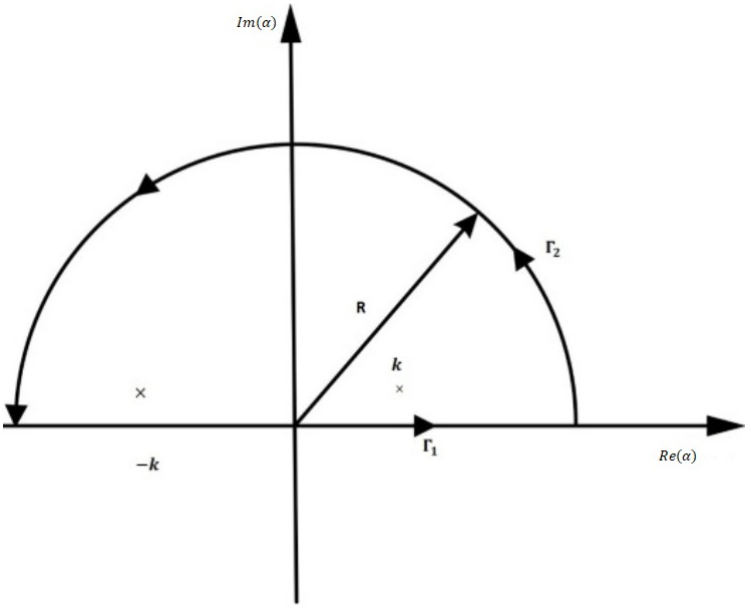

FIGURE 2.2: Contour plot in α plane

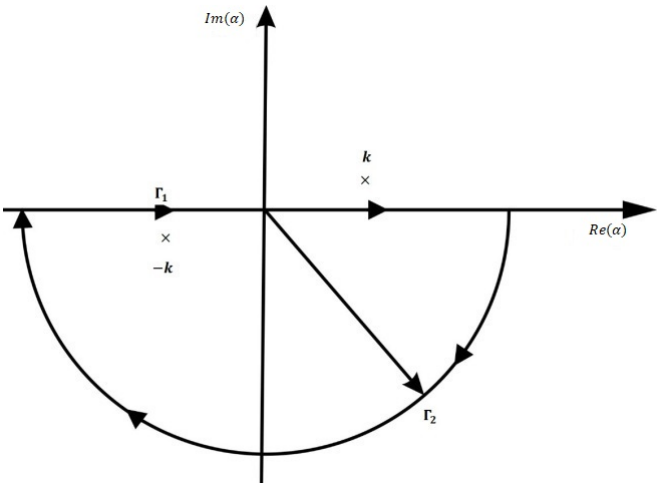

FIGURE 2.3: Contour plot in α plane

Using contour integration along paths Γ_1 and Γ_2 gives

$$\int_{\Gamma_1} f(\alpha)d\alpha + \int_{\Gamma_2} f(\alpha)d\alpha = 2\pi i Res f(\alpha) \quad \text{at} \quad \alpha = k. \tag{2.37}$$

Since

$$\int_{\Gamma_2} f(\alpha)d\alpha \longrightarrow 0 \text{ and } \int_{\Gamma_1} f(\alpha)d\alpha = \Phi(x, x') \text{ as } R \longrightarrow \infty$$

$$\Phi(x, x') = \frac{i}{2k} e^{ik(x-x')}. \tag{2.38}$$

When $x - x' < 0$, the semicircle in the lower half-plane is chosen for Γ_2 so as to make $\int_{\Gamma_2} f(\alpha)d\alpha \longrightarrow 0$, as shown in Fig.2(b). Counter integration gives

$$\Phi(x, x') = \frac{i}{2k} e^{-ik(x-x')}. \tag{2.39}$$

As a result, the one-dimensional free-space Green's function is represented as

$$\Phi(x, x') = \frac{i}{2k} e^{ik|x-x'|}. \tag{2.40}$$

Chapter 3

Sound Source Inclusion in Discontinuous Waveguide

In this chapter the discussion is about the propagation of acoustic waves in discontinuous waveguide. The boundaring wall conditions are assumed acoustical rigid. The boundary value problems involve Helmholtz's equation as governing equation along with rigid-rigid boundary conditions. Mode-matching technique has been used to tackle the problem. The numerical results contain the matching conditions of pressures and velocities at the interface. The propagation of reflected and transmitted energy fluxes by varying frequency. This chapter includes two problems. First problem consists of the case when duct regions comprises compressible fluid. While in the later case sound absorbent material is used.

3.1 Sound Source Excitation in Discontinuous Waveguide:

Consider acoustic wave propagation in rectangular waveguide having regions R_1 and R_2 that are bounded by rigid walls at $\bar{y} = \bar{0}, \bar{h}_1, \bar{h}_2$, when $\bar{x} > \bar{0}$, $\bar{x} < \bar{0}$ and at $\bar{x} = \bar{0}$ when $\bar{h}_1 \leq \bar{y} \leq \bar{h}_2$. Note that overbars here and throughout the thesis denote the dimensional setting of coordinates. The inside of the regions R_1 and

R_2 are filled with compressible fluid of density ρ having sound speed c. A sound source $\bar{Q}(\bar{x},\bar{y})$ in the duct R_1 at point $(\bar{x},\bar{y})=(\bar{a},\bar{b})$ is located. The geometry of problem is shown in Fig.1.

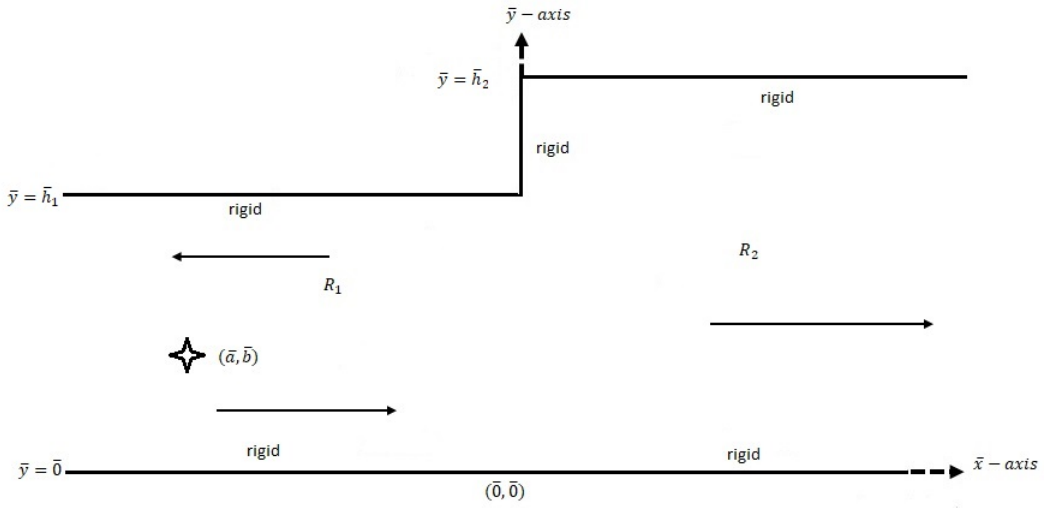

FIGURE 3.1: The geometry of the semi-infinite duct

The fluid potential in ducts R_1 and R_2 are represented by $\bar{\Phi}_1$ and $\bar{\Phi}_2$, respectively. Thus, the fluid potential $\bar{\Phi}(\bar{x},\bar{y})$ in the waveguide

$$\bar{\Phi}(\bar{x},\bar{y})=\begin{cases}\bar{\Phi}_1(\bar{x},\bar{y}), & \bar{x}<\bar{0},\quad \bar{0}\le\bar{y}\le\bar{h}_1,\\ \bar{\Phi}_2(\bar{x},\bar{y}), & \bar{x}>\bar{0},\quad \bar{0}\le\bar{y}\le\bar{h}_2.\end{cases} \tag{3.1}$$

At $(\bar{x},\bar{y})=(\bar{a},\bar{b})$ the fluid potential $\bar{\Phi}_1(\bar{x},\bar{y})$ satisfy the Helmholtz's equations

$$\left\{\frac{\partial^2}{\partial\bar{x}^2}+\frac{\partial^2}{\partial\bar{y}^2}+k^2\right\}\bar{\Phi}_1(\bar{x},\bar{y})=\bar{Q}(\bar{x},\bar{y}), \tag{3.2}$$

but when $(\bar{x},\bar{y})\neq(\bar{a},\bar{b})$ the fluid potential satisfies

$$\left\{\frac{\partial^2}{\partial\bar{x}^2}+\frac{\partial^2}{\partial\bar{y}^2}+k^2\right\}\bar{\Phi}_1(\bar{x},\bar{y})=0.$$

The fluid potential $\bar{\Phi}_2(\bar{x},\bar{y})$ satisfies the Helmholtz's equation

$$\left\{\frac{\partial^2}{\partial\bar{x}^2}+\frac{\partial^2}{\partial\bar{y}^2}+k^2\right\}\bar{\Phi}_2(\bar{x},\bar{y})=\bar{0}. \tag{3.3}$$

At rigid walls the normal velocity is zero, that gives

$$\frac{\partial \bar{\Phi}_1}{\partial \bar{y}} = \bar{0}, \quad \bar{y} = \bar{0}, \ \bar{h}_1, \tag{3.4}$$

$$\frac{\partial \bar{\Phi}_2}{\partial \bar{y}} = \bar{0}, \quad \bar{y} = \bar{0}, \ \bar{h}_2, \tag{3.5}$$

$$\frac{\partial \bar{\Phi}_2}{\partial \bar{x}} = \bar{0}, \quad \bar{x} = \bar{0}, \ \bar{h}_1 \leq \bar{x} \leq \bar{h}_2. \tag{3.6}$$

We make the problem dimensionless by using length scale k^{-1} and time scale ω^{-1} through the transformations

$$\begin{aligned} x &= k\bar{x}, \\ y &= k\bar{y}, \\ t &= \omega\bar{t}, \\ \frac{\partial}{\partial \bar{x}} &= k\frac{\partial}{\partial x}, \\ \frac{\partial^2}{\partial \bar{x}^2} &= k^2\frac{\partial^2}{\partial x^2}, \\ \Phi &= \frac{k^2}{\omega}\bar{\Phi}, \\ Q(x,y) &= \frac{k^2}{\omega}\bar{Q}(\bar{x},\bar{y}). \end{aligned} \tag{3.7}$$

Incorporating these transformations into (3.1)-(3.6) we get the dimensionless form of boundary value problem. The fluid potential in ducts R_1 and R_2 are represented by Φ_1 and Φ_2, respectively. Thus, the fluid potential $\Phi(x,y)$ in the waveguide

$$\Phi(x,y) = \begin{cases} \Phi_1(x,y), & x < 0, \quad 0 \leq y \leq h_1, \\ \Phi_2(x,y), & x > 0, \quad 0 \leq y \leq h_2. \end{cases} \tag{3.8}$$

At $(x,y) = (a,b)$ the fluid potential $\Phi_1(x,y)$ satisfy the Helmholtz's equations

$$\left\{ \frac{\partial^2}{\partial x^2} + \frac{\partial^2}{\partial y^2} + 1 \right\} \Phi_1(x,y) = Q(x,y), \tag{3.9}$$

but when $(x, y) \neq (a, b)$ the fluid potential satisfies

$$\left\{ \frac{\partial^2}{\partial x^2} + \frac{\partial^2}{\partial y^2} + 1 \right\} \Phi_1(x, y) = 0.$$

The fluid potential $\Phi_2(x, y)$ satisfies the Helmholtz's equation

$$\left\{ \frac{\partial^2}{\partial x^2} + \frac{\partial^2}{\partial y^2} + 1 \right\} \Phi_2(x, y) = 0. \tag{3.10}$$

The rigid wall conditions satisfy the following dimensionless form of boundary conditions

$$\frac{\partial \Phi_1}{\partial y} = 0, \quad y = 0,\ h_1, \quad x < 0, \tag{3.11}$$

$$\frac{\partial \Phi_2}{\partial y} = 0, \quad y = 0,\ h_2, \quad x > 0, \tag{3.12}$$

$$\frac{\partial \Phi_2}{\partial x} = 0, \quad x = 0,\ h_1 \leq x \leq h_2. \tag{3.13}$$

In next section we solve the boundary conditions.

3.2 Mode-Matching Solution

The Mode-matching technique is applied to solve the boundary value problem. First we determine the eigenfunction expansion of region R_1. In this region the fluid potential $\Phi_1(x, y)$ is the sum of incident field $\Phi_1^{\mathrm{i}}(x, y)$ and reflected field $\Phi_1^{\mathrm{r}}(x, y)$

$$\Phi_1(x, y) = \Phi_1^{\mathrm{i}}(x, y) + \Phi_1^{\mathrm{r}}(x, y). \tag{3.14}$$

For reflected field the governing equations are

$$\left\{ \frac{\partial^2}{\partial x^2} + \frac{\partial^2}{\partial y^2} + 1 \right\} \Phi_1^{\mathrm{r}}(x, y) = 0, \tag{3.15}$$

$$\frac{\partial \Phi_1^{\mathrm{r}}(x,y)}{\partial y} = 0, \quad \text{at} \quad y = 0, \quad h_1. \tag{3.16}$$

From superposition principle, the reflected field is the linear combination of reflected modes

$$\Phi_1^{\mathrm{r}}(x,y) = \sum_{n=0}^{\infty} A_n \Phi_{1n}(x,y), \tag{3.17}$$

where $A_n,\ n = 0, 1, 2, ...$ are the amplitudes of reflected modes and $\Phi_{1n}(x,y),\ n = 0, 1, 2, ...$ expresses the propagation modes.

To calculate $\Phi_{1n}(x,y),\ n = 0, 1, 2, ...,$ we use the separation of variables method to write

$$\Phi_{1n}(x,y) = X_{1n}(x)\psi_{1n}(y). \tag{3.18}$$

On substituting (3.18) into (3.15), we find two ordinary differential equations, that are solved to get

$$X_{1n}(x) = c_1 e^{i\eta_n x} + c_2 e^{-i\eta_n x} \tag{3.19}$$

and

$$\psi_{1n}(y) = c_3 \cos(\lambda_n y) + c_4 \sin(\lambda_n y), \tag{3.20}$$

where

$$\eta_n = \sqrt{1 - \lambda_n^2}.$$

Note that $X_{1n}(x)$ determines the propagation of n^{th} mode along x-direction and $\psi_{1n}(y)$ determines its shape in R_1. As we consider reflected wave towards x-direction only, therefore $c_1 = 0$. Also applying rigid boundary conditions (3.16), it is clear that $c_3 = 0$, for non-trivial solution $\lambda_n = \dfrac{n\pi}{h_1}$ and

$$\psi_{1n}(y) = \cos\left(\frac{n\pi}{h_1} y\right), \quad n = 0, 1, 2, ...$$

Since $\psi_{1n}(y) = \cos\left(\dfrac{n\pi}{h_1} y\right),\ n = 0, 1, 2, ...$ are orthogonal functions and satisfy the orthogonality relation

$$\int_0^{h_1} \psi_{1n}(y)\psi_{1m}(y)dy = \delta_{mn}\epsilon_m \frac{h_1}{2}, \tag{3.21}$$

where δ_{mn} is kronecker delta and is defined as

$$\delta_{mn} = \begin{cases} 1, & m = n, \\ 0, & \text{otherwise}, \end{cases}$$

$$\epsilon_m = \begin{cases} 2, & m = 0, \\ 1, & \text{otherwise}. \end{cases}$$

The orthonormal form of these eigenfunctions is

$$\varphi_{1n}(y) = \sqrt{\frac{2}{h_1 \epsilon_m}} \cos(\frac{n\pi}{h_1} y), \tag{3.22}$$

where

$$\int_0^{h_1} \varphi_{1n}(y)\varphi_{1m}(y)dy = \delta_{mn}. \tag{3.23}$$

Therefore, the reflected field (3.18) can be written as

$$\Phi_1^{\mathrm{r}}(x, y) = \sum_{n=0}^{\infty} A_n \varphi_{1n}(y) e^{-i\eta_n x}. \tag{3.24}$$

For source $Q(x, y) = -J\delta(x - a)\delta(y - b)$, we rewrite (3.9) as

$$\left\{ \frac{\partial^2}{\partial x^2} + \frac{\partial^2}{\partial y^2} + 1 \right\} \Phi_1^{\mathrm{i}}(x, y) = -J\delta(x - a)\delta(y - b), \tag{3.25}$$

subject to rigid boundary conditions

$$\frac{\partial \Phi_1^{\mathrm{i}}}{\partial y} = 0, \text{ at } \quad y = 0, \quad h_1, \tag{3.26}$$

where J is source strength that will be defined in numerical section.

To determine the solution of (3.25)-(3.26), we use eigenfunction expansion method. The response of sound source in semi-infinite duct can be expressed as

$$\Phi_1^{\mathrm{i}}(x, y) = \sum_{n=0}^{\infty} a_n(x) \varphi_{1n}(y), \tag{3.27}$$

where $a_n(x); n = 0, 1, 2, ...$ are unknowns. To find these, we substitute (3.27) into (3.25) to get

$$\sum_{n=0}^{\infty}\left\{\frac{d^2a_n(x)}{dx^2}+\eta_n^2a_n(x)\right\}\varphi_{1n}(y) = -J\delta(x-a)\delta(y-b). \tag{3.28}$$

Multiplying (3.28) by $\varphi_{1m}(y)$ and integrating from 0 to h_1, we obtain

$$\sum_{n=0}^{\infty}\left\{\frac{d^2a_n(x)}{dx^2}+\eta_n^2a_n(x)\right\}\int_0^{h_1}\varphi_{1n}(y)\varphi_{1m}(y)dy = -J\delta(x-a)\int_0^{h_1}\varphi_{1m}(y)\delta(y-b)dy. \tag{3.29}$$

On using the orthogonality relation (3.23) into (3.29), we achieve

$$\sum_{n=0}^{\infty}\left\{\frac{d^2a_n(x)}{dx^2}+\eta_n^2a_n(x)\right\}\delta_{mn} = -J\delta(x-a)\varphi_{1m}(b), \tag{3.30}$$

or

$$\frac{d^2a_m(x)}{dx^2}+\eta_m^2a_m(x) = -J\delta(x-a)\varphi_{1m}(b). \tag{3.31}$$

By using the Green's function (2.40) for free space, we reached at

$$a_m(x) = iJ\frac{\varphi_{1m}(b)}{2\eta_m}e^{i\eta_m|x-a|}. \tag{3.32}$$

Now putting (3.32) into (3.27), we achieve

$$\Phi_1^{\mathrm{i}}(x,y) = \sum_{n=0}^{\infty}iJ\frac{\varphi_{1n}(y)\varphi_{1n}(b)}{2\eta_n}e^{i\eta_n|x-a|}. \tag{3.33}$$

Finally, by combining (3.24) and (3.33), the total field in region R_1 is obtained as

$$\Phi_1(x,y) = iJ\sum_{n=0}^{\infty}\frac{\varphi_{1n}(y)\varphi_{1n}(b)}{2\eta_n}e^{i\eta_n|x-a|}+\sum_{n=0}^{\infty}A_n\varphi_{1n}(y)e^{-i\eta_nx}. \tag{3.34}$$

Similarly, for region R_2, the eigenfunction expansion form of transmitted duct modes is assumed as,

$$\Phi_2(x,y) = \sum_{n=0}^{\infty}B_n\Phi_{2n}(x,y), \tag{3.35}$$

where B_n; $n = 0, 1, 2, ...$, are transmitted modes amplitudes and $\Phi_{2n}(x, y)$ contains shape and direction of transmitted modes. To find $\Phi_{2n}(x, y)$ from boundary conditions for R_2, we use method of separation of variables. For this we assume

$$\Phi_{2n}(x, y) = X_{2n}(x)\psi_{2n}(y). \tag{3.36}$$

On substituting (3.36) into (3.10), we get

$$X_{2n}(x) = c_5 e^{is_n x} + c_6 e^{-is_n x} \tag{3.37}$$

and

$$\psi_{2n}(y) = c_7 \cos(\xi_n y) + c_8 \sin(\xi_n y), \tag{3.38}$$

where

$$s_n = \sqrt{1 - \xi_n^2}.$$

From rigid boundary conditions (3.12), $c_8 = 0$ and $\xi_n = \dfrac{n\pi}{h_2}$, $n = 0, 1, 2, ...$
Since $\psi_{2n}(y) = \cos\left(\dfrac{n\pi}{h_2} y\right)$; $n = 0, 1, 2, ...$ are orthogonal functions and satisfy the orthogonality relation

$$\int_0^{h_2} \cos(\frac{n\pi}{h_2} y) \cos(\frac{m\pi}{h_2} y) dy = \delta_{nm} \epsilon_m \frac{h_2}{2}. \tag{3.39}$$

The orthonormal form of these eigenfunctions is

$$\varphi_{2n}(y) = \sqrt{\frac{2}{\epsilon_m h_2}} \cos(\frac{n\pi}{h_2} y), \tag{3.40}$$

where

$$\int_0^{h_2} \varphi_{2n}(y)\varphi_{2m}(y) dy = \delta_{nm}. \tag{3.41}$$

As transmission takes place in positive x-direction only, therefore $c_6 = 0$ and transmitted field in R_2 can be given by

$$\Phi_2(x, y) = \sum_{n=0}^{\infty} B_n \varphi_{2n}(y) e^{is_n x}. \tag{3.42}$$

At matching interface $x = 0$, the continuity of acoustic pressure gives

$$\Phi_1(0, y) = \Phi_2(0, y), \quad 0 \leq y \leq h_1.$$

On substituting (3.34) and (3.42) into above equation, we have

$$iJ \sum_{n=0}^{\infty} \frac{\varphi_{1n}(y)\varphi_{1n}(b)}{2\eta_n} e^{i\eta_n|a|} + \sum_{n=0}^{\infty} A_n \varphi_{1n}(y) = \sum_{n=0}^{\infty} B_n \varphi_{2n}(y). \tag{3.43}$$

Multiplying (3.43) by $\varphi_{1m}(y)$ and integrating from 0 to h_1,

$$\begin{aligned} iJ \sum_{n=0}^{\infty} \frac{\varphi_{1n}(b)}{2\eta_n} e^{i\eta_n|a|} \int_0^{h_1} \varphi_{1n}(y)\varphi_{1m}(y)dy + \sum_{n=0}^{\infty} A_n \int_0^{h_1} \varphi_{1n}(y)\varphi_{1m}(y)dy \\ = \sum_{n=0}^{\infty} B_n \int_0^{h_1} \varphi_{2n}(y)\varphi_{1m}(y)dy. \end{aligned} \tag{3.44}$$

Substituting the orthogonality relation (3.23) into (3.44), we find

$$iJ \frac{\varphi_{1m}(b)}{2\eta_m} e^{i\eta_m|a|} + A_m = \sum_{n=0}^{\infty} B_n R_{nm}, \tag{3.45}$$

where

$$R_{nm} = \int_0^{h_1} \varphi_{2n}(y)\varphi_{1m}(y)dy.$$

Now using the normal velocity condition at interface $x = 0$

$$\Phi_{2x}(0, y) = \begin{cases} \Phi_{1x}(0, y), & 0 \leq y \leq h_1, \\ 0, & h_1 \leq y \leq h_2. \end{cases} \tag{3.46}$$

On invoking (3.34) and (3.42) into (3.46), we achieve

$$\sum_{n=0}^{\infty} is_n \varphi_{2n}(y) = \begin{cases} -J \sum_{n=0}^{\infty} \frac{\varphi_{1n}(y)\varphi_{1n}(b)e^{i\eta_n|a|}}{2} (\frac{-a}{|a|}) \\ -\sum_{n=0}^{\infty} A_n \varphi_{1n}(y) i\eta_n, & 0 \leq y \leq h_1, \\ 0, & h_1 \leq y \leq h_2. \end{cases} \tag{3.47}$$

Multiplying by $\varphi_{2m}(y)$ and integrating from 0 to h_2, we get

$$\sum_{n=0}^{\infty} B_n i s_n \int_0^{h_2} \varphi_{2n}(y)\varphi_{2m}(y)dy = -J\sum_{n=0}^{\infty} \frac{\varphi_{1n}(b)}{2} e^{i\eta_n|a|}(\frac{-a}{|a|}) \int_0^{h_2} \varphi_{1n}(y)\varphi_{2m}(y)dy - \sum_{n=0}^{\infty} A_n i\eta_n \int_0^{h_2} \varphi_{2m}(y)\varphi_{1n}(y)dy. \tag{3.48}$$

On invoking the orthogonality relation (3.41) into (3.48), we find

$$B_m i s_m = -J\sum_{n=0}^{\infty} \frac{\varphi_{1n}(b)}{2} e^{i\eta_n|a|}(\frac{-a}{|a|})R_{nm} - \sum_{n=0}^{\infty} A_n i\eta_n R_{nm}, \tag{3.49}$$

where

$$R_{nm} = \int_0^{h_2} \varphi_{1n}(y)\varphi_{2m}(y)dy.$$

By fixing $m = n = 0, 1, 2, ...N$, we get $2(N+1)$ number of equations with $2(N+1)$ unknowns. These are solved simultaneously to get these unknowns.

3.3 Energy Fux

The energy flux/power in closed region can be defined as [69]

$$\text{Energy flux} = \frac{1}{2}\Re\left[i\int_\Omega \Phi(\frac{\partial\Phi}{\partial x})^* d\Omega\right], \tag{3.50}$$

where $\Re$ denotes real part and Ω is the domain of region. The transmission loss is defined as [70]

$$TL = -20\log\left[\frac{P_t}{P_i}\right]. \tag{3.51}$$

The incident and reflected power in region R_1 can be found by using (3.34) into (3.50),

$$\text{Energy flux}|_{R_1} = \frac{1}{2}\Re\sum_{n=0}^{\infty}\sum_{m=0}^{\infty}\left[-i|J|^2\frac{\varphi_{1n}(b)\varphi_{1m}(b)}{4\eta_n}e^{i|x-a|(\eta_n-\eta_m^*)}\frac{x-a}{|x-a|}\right.$$
$$+\frac{J\varphi_{1n}(b)A_m^*\eta_m^*}{2\eta_n}e^{i\eta_n|x-a|}e^{i\eta_m^* x}-\frac{iJ^*A_n\varphi_{1m}(b)}{2}e^{-i\eta_m^*|x-a|}e^{-i\eta_n x}\frac{x-a}{|x-a|}$$
$$\left.-A_nA_m^*e^{ix(\eta_m^*-\eta_n)}\right]\int_0^{h_1}\varphi_{1n}(y)\varphi_{1m}(y)dy. \quad (3.52)$$

On using orthogonality relation (3.23) into (3.52), we achieved

$$\text{Energy flux}|_{R_1} = \frac{1}{2}\Re\sum_{m=0}^{\infty}\left[|J|^2\frac{|\varphi_{1m}(b)|^2}{4\eta_m}e^{i|x-a|(\eta_m-\eta_m^*)}\frac{x-a}{|x-a|}\right]-$$
$$\frac{1}{2}\Re\sum_{m=0}^{\infty}\left[A_m|^2\eta_m^\star e^{-ix(\eta_m-\eta_m^*)}+J\frac{\varphi_{1m}(b)}{2\eta_m}e^{i\eta_m|x-a|}e^{i\eta_m^* x}A_m^*\eta_m^*+\right.$$
$$\left.iJ^*\varphi_{1m}(b)A_me^{-i\eta_m x}e^{-i\eta_m^*|x-a|}\frac{x-a}{|x-a|}\right], \quad (3.53)$$

or

$$\text{Energy flux}|_{R_1} = P_i - P_r, \quad (3.54)$$

where

$$P_i = \frac{1}{2}\Re\sum_{m=0}^{\infty}\left[|J|^2\frac{|\varphi_{1m}(b)|^2}{4\eta_m}e^{i|x-a|(\eta_m-\eta_m^*)}\frac{x-a}{|x-a|}\right] \quad (3.55)$$

and

$$P_r = \frac{1}{2}\Re\sum_{m=0}^{\infty}\left[A_m|^2\eta_m^\star e^{-ix(\eta_m-\eta_m^*)}+J\frac{\varphi_{1m}(b)}{2\eta_m}e^{i\eta_m|x-a|}e^{i\eta_m^* x}A_m^*\eta_m^*+\right.$$
$$\left.iJ^*\varphi_{1m}(b)A_me^{-i\eta_m x}e^{-i\eta_m^*|x-a|}\frac{x-a}{|x-a|}\right]. \quad (3.56)$$

Likewise, for energy flux in R_2, we substitute (3.42) into (3.50) which finally yields

$$\text{Energy flux}|_{R_2} = \frac{1}{2}\Re\left(\sum_{n=0}^{\infty}|B_n|^2 s_n\right). \quad (3.57)$$

or

$$\text{Energy flux}|_{R_2} = P_t. \quad (3.58)$$

From the conservation of energy law

$$\text{Energy flux}|_{R_1} = \text{Energy flux}|_{R_2}, \tag{3.59}$$

which yield

$$P_i - P_r = P_t, \tag{3.60}$$

or

$$P_i = P_r + P_t. \tag{3.61}$$

To scale the power at unity we divide (3.61) with P_i, then

$$1 = E_r + E_t, \tag{3.62}$$

where

$$E_r = \frac{P_r}{P_i} \quad \text{and} \quad E_t = \frac{P_t}{P_i}. \tag{3.63}$$

Note that we can achieve (3.61) using (3.45) and (3.49). To get this, we rewrite (3.45) as

$$B_m s_m = J \sum_{n=0}^{\infty} \frac{\varphi_{1n}(b)}{2i} e^{i\eta_n|a|} \frac{a}{|a|} R_{nm} - \sum_{n=0}^{\infty} A_n \eta_n R_{nm}. \tag{3.64}$$

On multiplying (3.64) by $\sum_{m=0}^{\infty} B_m^{\star}$, we get

$$\sum_{m=0}^{\infty} |B_m|^2 s_m = J \sum_{n=0}^{\infty} \frac{\varphi_{1n}(b)}{2i} e^{i\eta_n|a|} \frac{a}{|a|} \sum_{m=0}^{\infty} B_m^{\star} R_{nm} - \sum_{n=0}^{\infty} A_n \eta_n \sum_{m=0}^{\infty} B_m^{\star} R_{nm}. \tag{3.65}$$

Taking conjugate of (3.45), we get

$$-iJ \frac{\varphi_{1n}(b)}{2\eta_n^*} e^{-i\eta_n^*|a|} + A_n^* = \sum_{m=0}^{\infty} B_m^* R_{nm}. \tag{3.66}$$

By substituting (3.66) into (3.65) and taking real part, we obtain

$$\frac{1}{2}\Re\left[\sum_{m=0}^{\infty} |B_m|^2 s_m + \sum_{m=0}^{\infty} \eta_m |A_m|^2 + iJ \sum_{n=0}^{\infty} A_n^* \eta_n^* \frac{\varphi_{1n}(b)}{2\eta_n} e^{-i\eta_n|a|} + iJ \sum_{n=0}^{\infty} A_n \frac{\varphi_{1n}(b)}{2} e^{i\eta_n^{\star}|a|}\right] = \frac{1}{2}\Re\left[J^2 \sum_{n=0}^{\infty} \frac{\varphi_{1n}^2(b)}{4\eta_n^{\star}} e^{i(\eta_n - \eta_n^{\star})|a|} \frac{a}{|a|}\right], \tag{3.67}$$

or

$$P_i = P_r + P_t. \tag{3.68}$$

To scale the power at unity, we divide (3.68) with P_i, which yields 3.62,

$$1 = E_r + E_t.$$

Now to calculate transmission loss we use (3.55) into (3.51), we achieve

$$TL = -20 \log \left[\sum_{n=0}^{\infty} \frac{4|B_n|^2 s_n \eta_n}{|J|^2 |\varphi_{1n}(b)|^2} \right] \tag{3.69}$$

3.4 Sound Source in Discontinuous Waves Involving Porous Material

The basic structure of the waveguide is same as discussed in section 1. However, the region between $h_1 \leq y \leq h_2$ at $x \geq 0$ contains sound absorbent material. The physical configuration of the waveguide is shown in Fig.2.

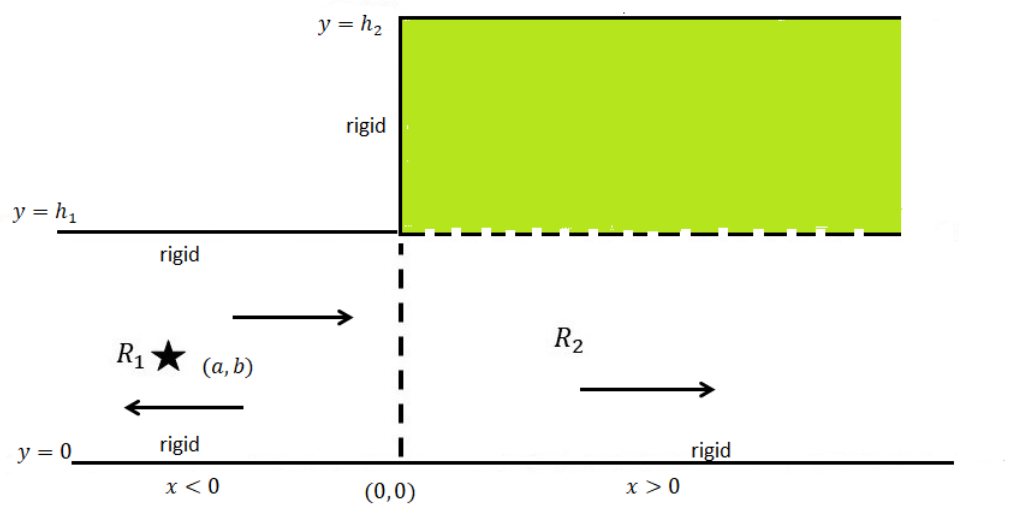

FIGURE 3.2: The geometry of the semi-infinite duct

The governing differential system is made dimensionless through transformation as explained in section 1. The non-dimensional fluid potential $\Phi(x, y)$ in waveguide

is

$$\Phi(x,y) = \begin{cases} \Phi_1(x,y), & x<0, \quad 0 \le y \le h_1, \\ \Phi_2(x,y), & x>0, \quad 0 \le y \le h_2. \end{cases} \tag{3.70}$$

The governing Helmholtz's equation in R_1 satisfies at $x=a$ and $y=b$,

$$\left\{\frac{\partial^2}{\partial x^2}+\frac{\partial^2}{\partial y^2}+1\right\}\Phi_1^{\mathrm{i}}(x,y) = -J\delta(x-a)\delta(y-b), \tag{3.71}$$

while at $x \neq a$ and $y \neq b$,

$$\left\{\frac{\partial^2}{\partial x^2}+\frac{\partial^2}{\partial y^2}+1\right\}\Phi_1^{\mathrm{r}}(x,y) = 0.$$

The rigid boundary conditions are

$$\frac{\partial \Phi_1}{\partial y} = 0, \qquad y = 0,\ h_1. \tag{3.72}$$

Since first duct is same as in previous problem, so $\Phi_1(x,y)$ will be same, i.e.

$$\Phi_1(x,y) = iJ\sum_{n=0}^{\infty}\frac{\varphi_{1n}(y)\varphi_{1n}(b)}{2\eta_n}e^{i\eta_n|x-a|} + \sum_{n=0}^{\infty}A_n\varphi_{1n}(y)e^{-i\eta_n x}. \tag{3.73}$$

The fluid potential $\Phi_2(x,y)$ in region R_2 satisfies

$$\left\{\frac{\partial^2}{\partial x^2}+\frac{\partial^2}{\partial y^2}+1\right\}\Phi_2(x,y) = 0,\ x>0, \quad 0 \le y \le h_1, \tag{3.74}$$

in air medium and satisfies

$$\left\{\frac{\partial^2}{\partial x^2}+\frac{\partial^2}{\partial y^2}+\Gamma^2\right\}\Phi_2(x,y) = 0, \quad x>0, \quad h_1 \le y \le h_2, \tag{3.75}$$

in porous medium, where Γ is the non-dimensional propagation constant and is

$$\Gamma = 1 + ia_1\xi^{a_2} + a_3\xi^{a_4}. \tag{3.76}$$

The normalized complex density in non-dimensional form is given by

$$\beta = \Gamma\left(1 + a_5\xi^{a_6} - ia_7\xi^{a_8}\right). \tag{3.77}$$

Here,

$\xi = \dfrac{f\rho}{\sigma}$, is the non-dimensional parametric frequency in porous medium,

$\sigma = A_1\rho_b^{A_2}$, is the flow resistivity,

ρ_b is bulk density and f is the excitation frequency,

the constants $a_1, a_2, ..., a_8$ and $A_1 - A_2$ are determined experimentally and for different porous material their values are different.

The walls at $y = 0,\ h_2$ are acoustically rigid,

$$\frac{\partial\Phi_2}{\partial y} = 0, \qquad y = 0,\quad h_2. \tag{3.78}$$

At porous lining $y = h_1$, the velocities across the region are continuous

$$\frac{\partial\Phi_2}{\partial y}(x, h_1^+) = \frac{\partial\Phi_2}{\partial y}(x, h_1^-), \quad x > 0. \tag{3.79}$$

The continuity of pressures across the region is

$$\beta\Phi_2(x, h_1^+) = \Phi_2(x, h_1^-). \tag{3.80}$$

The eigenfunction expansion ansatz in region R_2 is

$$\Phi_{2n}(x, y) = \sum_{n=0}^{\infty} B_n Y_n(y) e^{is_n x}, \tag{3.81}$$

where $Y_n(y)$ the eigenfunctions that determine the shape of propagating modes, s_n be the n^{th} mode wavenumber and B_n is the n^{th} mode amplitude. We define

$$Y_n(y) = \begin{cases} Y_{1n}(y), & x > 0,\quad 0 \le y \le h_1, \\ Y_{2n}(y), & x > 0,\quad h_1 \le y \le h_2, \end{cases} \tag{3.82}$$

and then use (3.81) into (3.72)-(3.80) to get

$$Y''_{1n}(y) - \gamma_n^2 Y_{1n}(y) = 0, \quad 0 \leq y \leq h_1, \tag{3.83}$$

$$Y''_{2n}(y) - \lambda_n^2 Y_{1n}(y) = 0, \quad h_1 \leq y \leq h_2, \tag{3.84}$$

where

$$\gamma_n = \sqrt{s_n^2 - 1} \quad \text{and} \quad \lambda_n = \sqrt{s_n^2 - \Gamma^2}. \tag{3.85}$$

The boundary conditions are

$$Y'_{1n}(0) = 0, \tag{3.86}$$

$$Y'_{2n}(0) = 0, \tag{3.87}$$

$$Y'_{1n}(h_1) = Y'_{2n}(h_1), \tag{3.88}$$

$$Y_{1n}(h_1) = \beta Y_{2n}(h_1). \tag{3.89}$$

On solving (3.83) and (3.84), we find that

$$Y_{1n}(y) = c_9 \cosh(\gamma_n y) + c_{10} \sinh(\gamma_n y), \tag{3.90}$$

$$Y_{2n}(y) = c_{11} \cosh(\lambda_n y) + c_{12} \sinh(\lambda_n y). \tag{3.91}$$

By using (3.90) into (3.86), we find $c_{10} = 0$ then

$$Y_{1n}(y) = c_9 \cosh(\gamma_n y). \tag{3.92}$$

Accordingly on using (3.91) into (3.87), we get

$$c_{12} = -\frac{c_{11} \sinh(\lambda_n h_2)}{\cosh(\lambda_n h_2)}. \tag{3.93}$$

On using (3.93) into (3.91), we have

$$Y_{2n}(y) = -\frac{c_{11}}{\cosh(\lambda_n h_2)} \cosh\left[\lambda_n (y - h_2)\right]. \tag{3.94}$$

By using (3.92) and (3.94), (3.88) implies

$$c_{11} = \frac{c_9 \gamma_n \sinh(\gamma_n h_1) \cosh(\lambda_n h_2)}{\lambda_n \sinh\left[\lambda_n (h_2 - h_1)\right]}. \tag{3.95}$$

By using (3.95), (3.94) becomes

$$Y_{2n}(y) = -\frac{c_9 \gamma_n \sinh(\gamma_n h_1) \cosh\left[\lambda_n (y - h_2)\right]}{\lambda_n \sinh\left[\lambda_n (h_2 - h_1)\right]}. \tag{3.96}$$

Now on substituting (3.95) and (3.96) into (3.89), for non-trivial solution we get

$$\cosh(\gamma_n h_1) + \frac{\beta \gamma_n \sinh(\gamma_n h_1) \cosh\left[\lambda_n (h_2 - h_1)\right]}{\lambda_n \sinh\left[\lambda_n (h_2 - h_1)\right]} = 0. \tag{3.97}$$

Note that we can solve (3.97) numerically for s_n which yields λ_n and γ_n. The resulting eigenfunctions satisfy the following orthogonality relation,

$$\int_0^{h_1} Y_{1m}(y) Y_{1n}(y) dy + \beta \int_{h_1}^{h_2} Y_{2m}(y) Y_{2n}(y) dy = \delta_{mn} G_m, \tag{3.98}$$

where

$$G_m = \int_0^{h_1} Y_{1m}^2(y) dy + \beta \int_{h_1}^{h_2} Y_{2m}^2(y) dy. \tag{3.99}$$

On using (3.92) and (3.96) into (3.82), we get

$$Y_n(y) = \begin{cases} \cosh(\gamma_n y), & x > 0, \quad 0 \le y \le h_1, \\ -\dfrac{\gamma_n \sinh(\gamma_n h_1) \cosh\left[\lambda_n (h_2 - y)\right]}{\lambda_n \sinh\left[\lambda_n (h_2 - h_1)\right]}, & x > 0, \quad h_1 \le y \le h_2. \end{cases} \tag{3.100}$$

At matching interface $x = 0$, the continuity of acoustic pressure gives

$$\Phi_1(0, y) = \Phi_2(0, y), \quad 0 \le y \le h_1. \tag{3.101}$$

On using (3.73) and (3.81) into (3.101), we find

$$iJ\sum_{n=0}^{\infty}\frac{\varphi_{1n}(y)\varphi_{1n}(b)}{2\eta_n}e^{i\eta_n|-a|}+\sum_{n=0}^{\infty}A_n\varphi_{1n}(y)=\sum_{n=0}^{\infty}B_nY_n(y),\quad 0\le y\le h_1. \tag{3.102}$$

Multiplying with $\varphi_{1m}(y)$, integrating from 0 to h_1, we achieve

$$Q_m^i+\sum_{n=0}^{\infty}A_n\delta_{mn}=\sum_{n=0}^{\infty}B_nR_{mn}, \tag{3.103}$$

where

$$Q_m^i=iJ\frac{\varphi_{1m}(b)}{2\eta_m}e^{i\eta_m|-a|}, \tag{3.104}$$

and

$$R_{mn}=\int_0^{h_1}Y_n(y)\varphi_{1m}(y)dy. \tag{3.105}$$

On solving (3.103), we get

$$A_m=-Q_m^i+\sum_{n=0}^{\infty}B_nR_{mn}. \tag{3.106}$$

At matching interface $x=0$ the continuity of acoustic velocity gives

$$\Phi_{2x}(0,y)=\begin{cases}\Phi_{1x}(0,y), & 0\le y\le h_1,\\ 0, & h_1\le y\le h_2.\end{cases} \tag{3.107}$$

On using (3.73) and (3.81) into (3.107), multiplying with $Y_{2m}(y)$, integrating over $h_1\le y\le h_2$,

$$\sum_{n=0}^{\infty}\int_{h_1}^{h_2}\Phi_{2x}(0,y)Y_{2m}(y)dy=0. \tag{3.108}$$

Accordingly, on substituting (3.73) and (3.81) into (3.107), multiply with $Y_{1m}(y)$, integrating over $0\le y\le h_1$ to get

$$\begin{aligned}\sum_{n=0}^{\infty}\int_0^{h_1}\Phi_{2x}(0,y)Y_{1m}(y)dy=&-\int_0^{h_1}J\sum_{n=0}^{\infty}\frac{\varphi_{1n}(y)\varphi_{1n}(b)}{2}e^{i\eta_n|-a|}Y_{1m}(y)dy\\&-\sum_{n=0}^{\infty}A_ni\eta_n\int_0^{h_1}\varphi_{1n}(y)Y_{1m}(y)dy.\end{aligned} \tag{3.109}$$

Multiplying (3.108) with β and then adding the resulting to (3.109), we find

$$i\sum_{n=0}^{\infty} s_n \left[\int_0^{h_1} Y_{1n}Y_{1m}dy + \beta\int_{h_1}^{h_2} Y_{2m}Y_{2n}dy\right] B_n = P_m^i - i\sum_{n=0}^{\infty} A_n\eta_n R_{nm}. \quad (3.110)$$

On using orthogonality relation (3.98), we get

$$i\sum_{n=0}^{\infty} s_n B_n G_n \delta_{mn} = P_m^i - i\sum_{n=0}^{\infty} A_n\eta_n R_{nm}, \quad (3.111)$$

or

$$B_m = \frac{P_m^i}{is_m G_m} - \frac{1}{s_m G_m}\sum_{n=0}^{\infty} A_n\eta_n R_{nm}, \quad (3.112)$$

where

$$P_m^i = -J\sum_{n=0}^{\infty} \frac{\varphi_{1n}(b)}{2} e^{i\eta_n|-a|} R_{nm}. \quad (3.113)$$

By fixing $m = n = 0, 1, 2, ...N$, we get $2(N+1)$ number of equations with $2(N+1)$ unknowns. These are solved simultaneously to get these unknowns.

3.5 Numerical Results

In this section the above system of infinite linear algebraic equations (3.49) is truncated upto $n = 0, 1, 2, ..., N$ terms and then system is solved numerically. Note that the reduced system contains $2(N + 1)$ equations. By solving these equations, we obtain the coefficients $A_n, B_n, n = 0, 1, 2, ..., N$. Once these scattered coefficients are known the pressures and velocities can be plotted at interface. In order to show the graphs, fixing the duct heights at $h_1 = 0.25m$ and $h_2 = 0.35m$, the pressures and normal velocities components are plotted against non-dimensional duct heights at interface in figures 3.3-3.8. The physical parameters, $c = 343.5m/s$ and $\rho = 1.2043kg/m$.Note that the source is placed at $a = -0.2m$ and $b = 0.03m$ with strength $J = 500$.

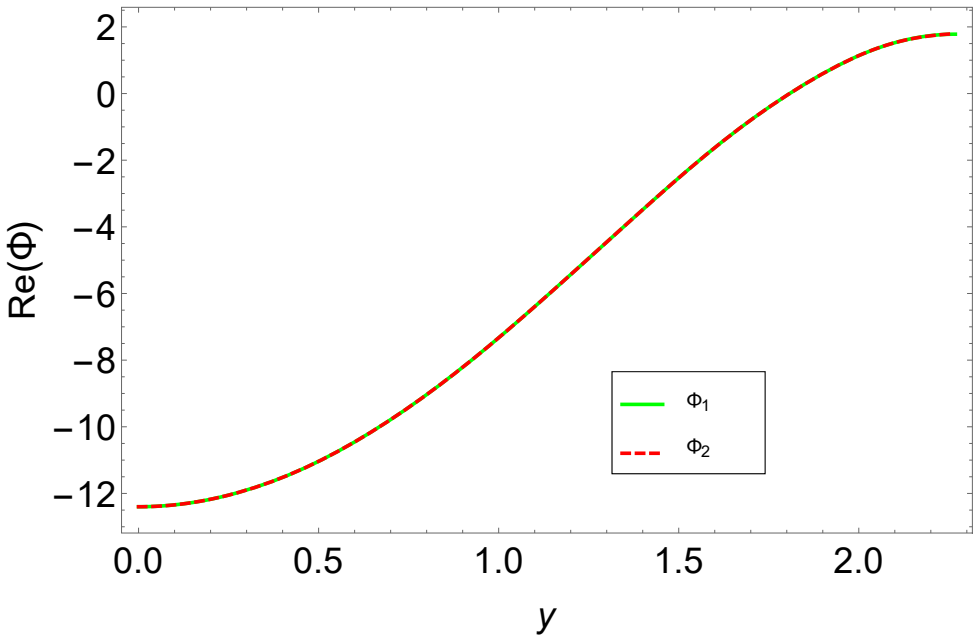

FIGURE 3.3: Real part of pressures $\Phi_1(0, y)$ and $\Phi_2(0, y)$, plotted against y, where $N = 20$ terms.

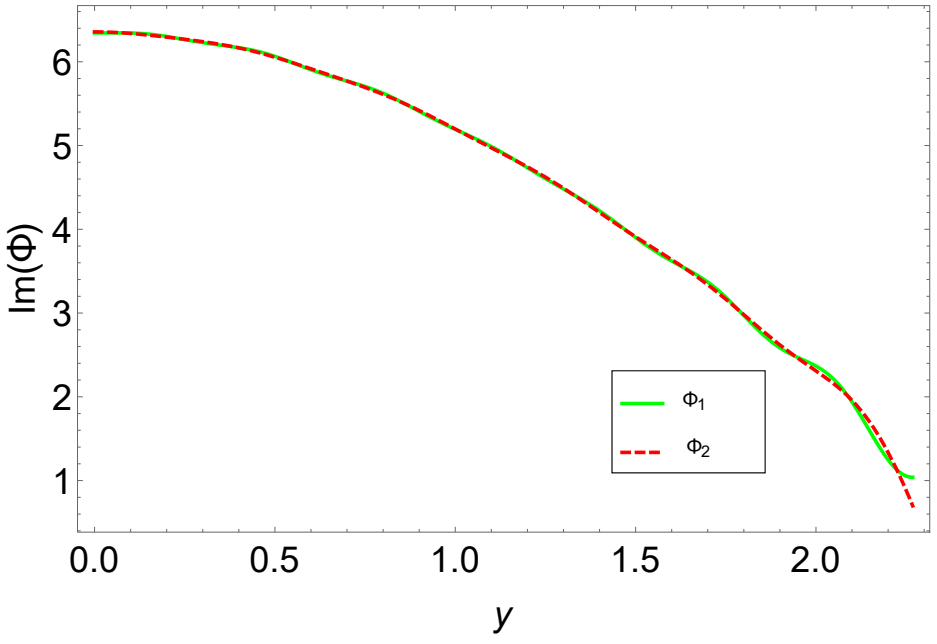

FIGURE 3.4: Imaginary part of pressures $\Phi_1(0, y)$ and $\Phi_2(0, y)$, plotted against y, where $N = 20$ terms.

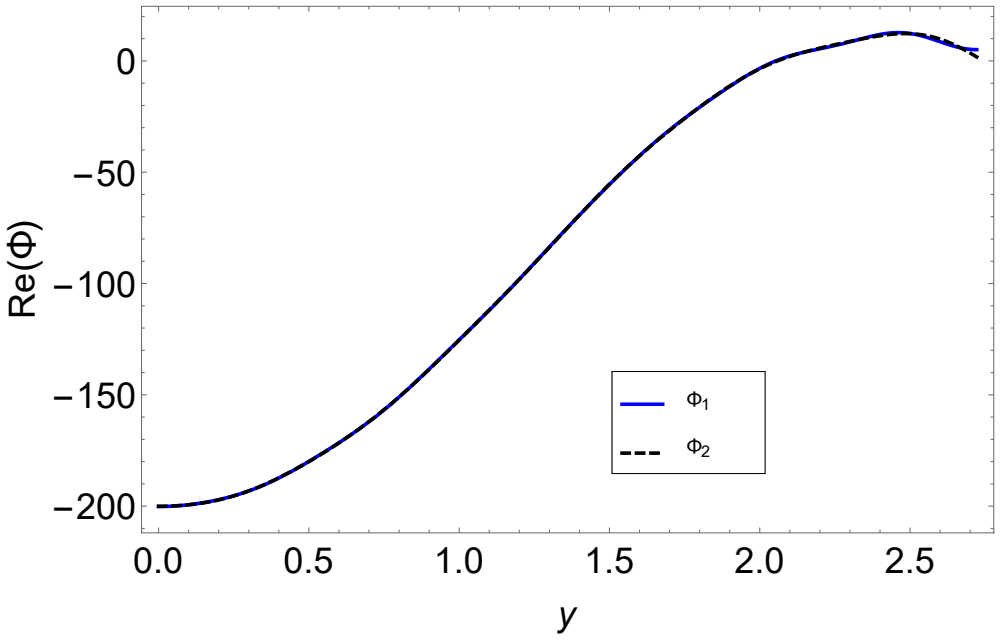

FIGURE 3.5: Real part of pressures $\Phi_1(0, y)$ and $\Phi_2(0, y)$, plotted against y, where $N = 10$ terms, $h_1 = 0.30$, $h_2 = 0.40$ and $J = 600$.

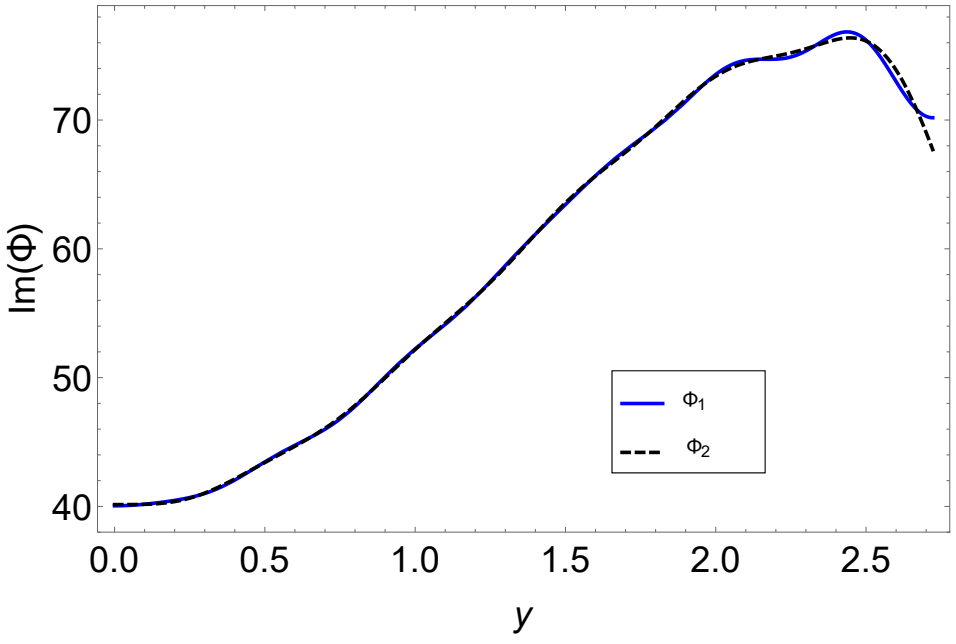

FIGURE 3.6: Imaginary part of pressures $\Phi_1(0, y)$ and $\Phi_2(0, y)$, plotted against y, where $N = 10$ terms $h_1 = 0.30$, $h_2 = 0.40$ and $J = 600$.

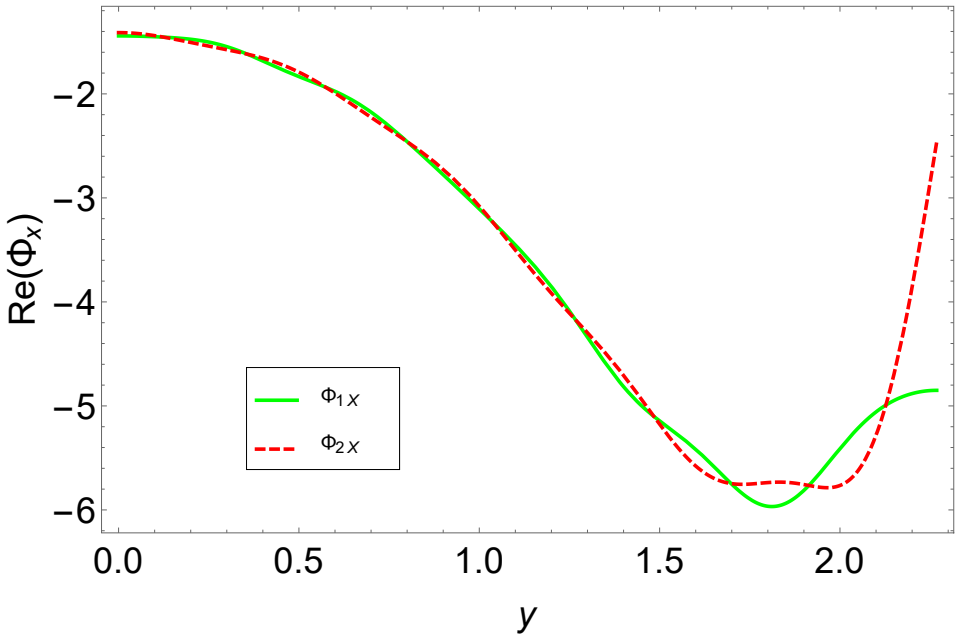

FIGURE 3.7: Real part of velocities $\Phi_{1x}(0, y)$ and $\Phi_{2x}(0, y)$, plotted against y, where $N = 20$ terms.

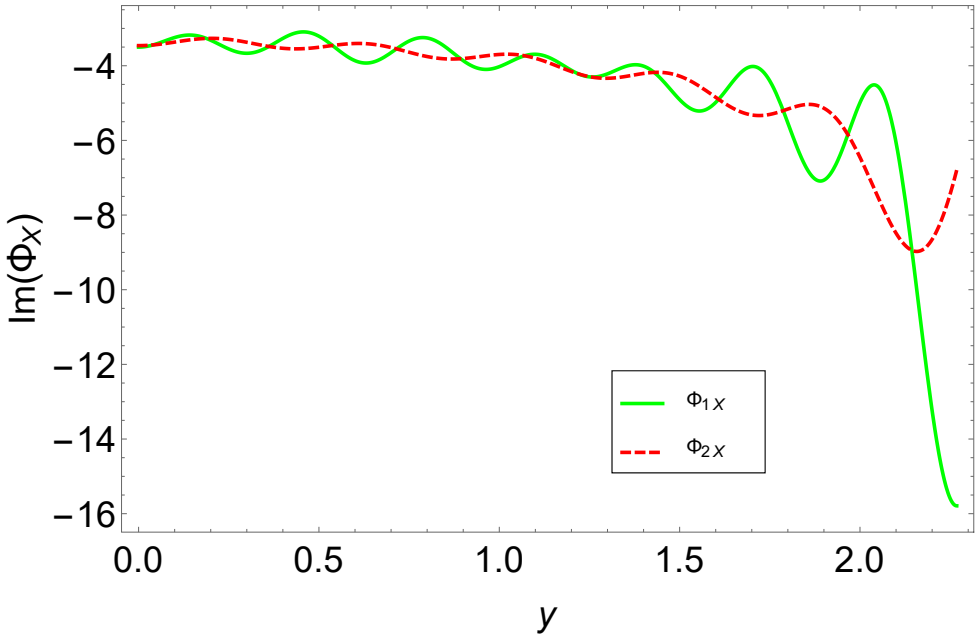

FIGURE 3.8: Imaginary part of velocities $\Phi_{1x}(0, y)$ and $\Phi_{2x}(0, y)$, plotted against y, where $N = 20$ terms.

Figs. 3.3 and 3.4 show the real and imaginary parts of pressures $\Phi_1(0, y)$ and $\Phi_2(0, y)$ in the regions $0 \leq y \leq h_1$ and $0 \leq y \leq h_2$, respectively. The real and imaginary parts of normal velocities $\Phi_{1x}(0, y)$ and $\Phi_{2x}(0, y)$ for the respective regions are plotted in Figs. 3.7 and 3.8. It can be observed from figures that the pressures and velocities in fluid regions agree very well. It shows that the truncated terms of solution satisfy the matching conditions.

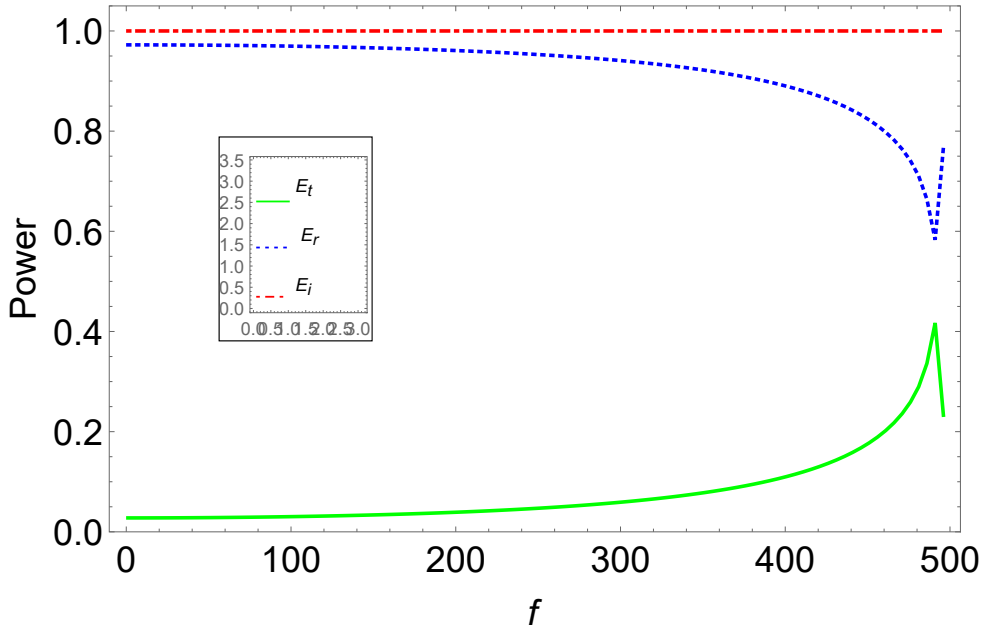

FIGURE 3.9: The energy flux/power components against frequency in discontinous waveguide with ducts hight $h_1 = 0.25$ and $h_2 = 0.35$ with $J = 30$.

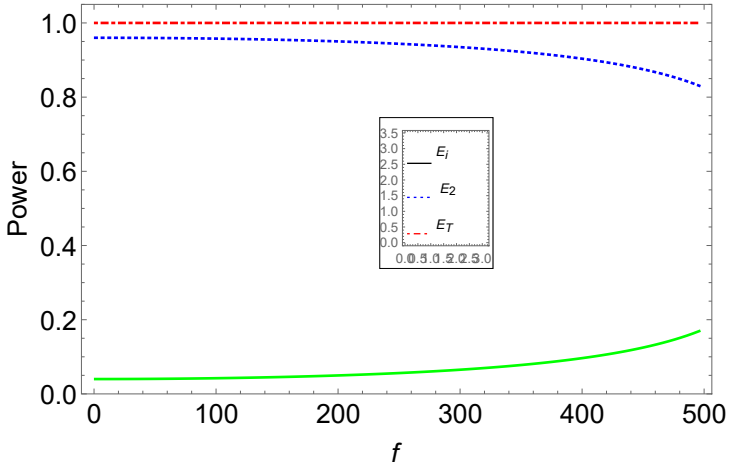

FIGURE 3.10: The energy flux/power components against frequency in discontinous waveguide with ducts hight $h_1 = 0.20$ and $h_2 = 0.30$ with $J = 100$.

In Figs. 3.9 and 3.10 the reflected power is shown by blue dotted curve, while green curve represents the transmitted power. The red dotted line is the sum of reflected and transmitted powers and which is unity.

Likewise, for porous material case the physical parameters can be chosen as $f = 100Hz, \rho = 1.2043kg/m^3, \rho_b = 100$ and coefficients for bulk acoustic properties for A glass, E glass, Basalt wool and Steel wool are shown in Table 3.1 [67]. Coefficients for the steady flow resistivity are shown in Table 3.2 [68]. For porous material case we have displayed Figs. 3.11-3.14 to show the real and imaginary parts of non-dimensional pressures and velocities at matching interface. Figs. 3.11 and 3.12 show the real and imaginary parts of pressures $\Phi_1(0, y)$ and $\Phi_2(0, y)$ in the region $0 \leq y \leq h_1$ and $0 \leq y \leq h_2$ respectively. The real and imaginary parts of normal velocities $\Phi_{1x}(0, y)$ and $\Phi_{2x}(0, y)$ for respective regions are shown in Figs. 3.13 and 3.14. From figures we can see that the pressures and velocities in fluid regions agree very well. It shows that the truncated terms of solution satisfy the matching conditions.

TABLE 3.1: Coefficients for bulk acoustic properties [73]

	A glass	**E glass**	**Basalt wool**	**Steel wool**
a_1	0.2251	0.2202	0.2178	0.1540
a_2	-0.5827	-0.5850	-0.6051	-0.7093
a_3	0.1443	0.2010	0.1281	0.1328
a_4	-0.7088	-0.5829	- 0.6746	-0.5571
a_5	-0.7177	-0.6687	-0.7664	-0.5557
a_7	0.1457	0.1689	0.1376	0.0876
a_8	-0.5951	-0.5707	-0.6276	-0.7609

TABLE 3.2: Coefficients for the steady flow resistivity [73]

	A glass	**E glass**	**Basalt wool**	**Steel wool**
A_1	1.857	5.774	3.012	0.312
A_2	1.687	1.792	1.761	1.615

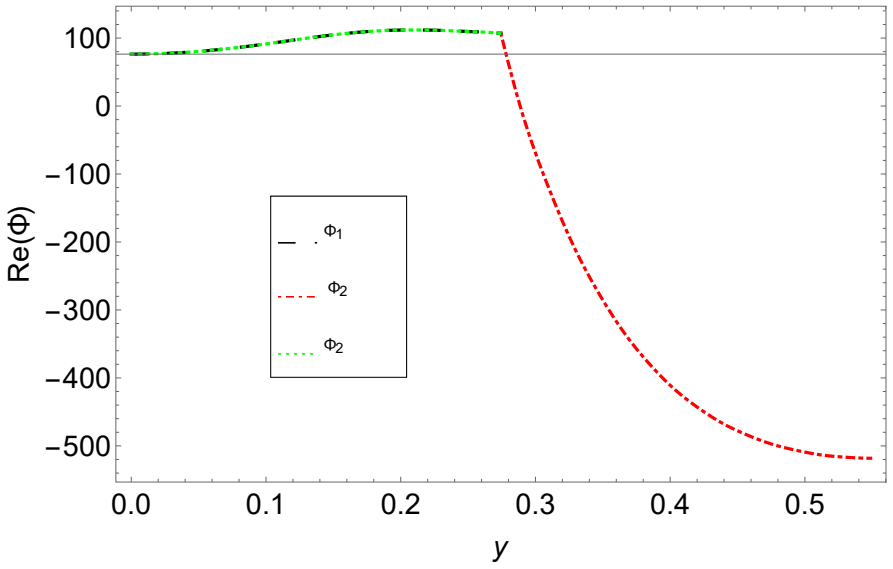

FIGURE 3.11: Real part of pressures $\Phi_1(0, y)$ and $\Phi_2(0, y)$, plotted against y, where $N = 15$ terms.

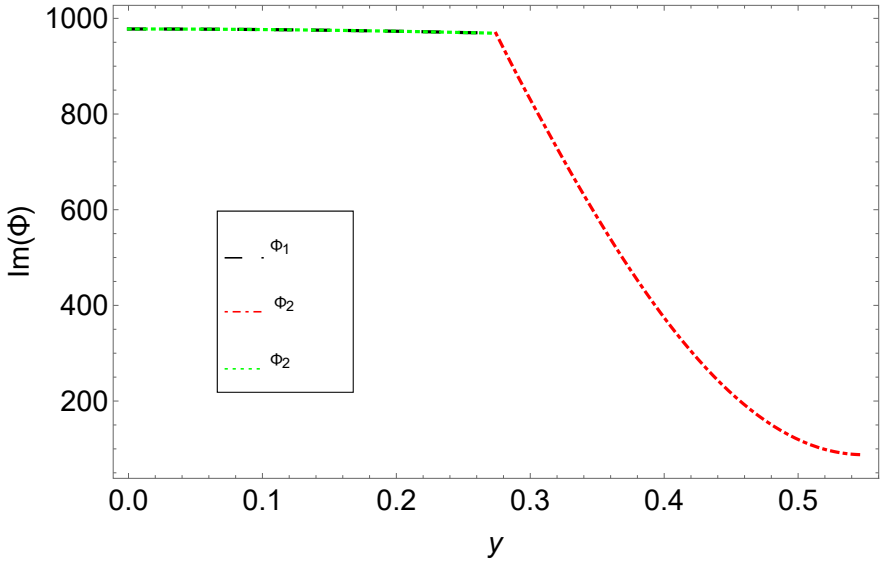

FIGURE 3.12: Real part of pressures $\Phi_1(0, y)$ and $\Phi_2(0, y)$, plotted against y, where $N = 15$ terms.

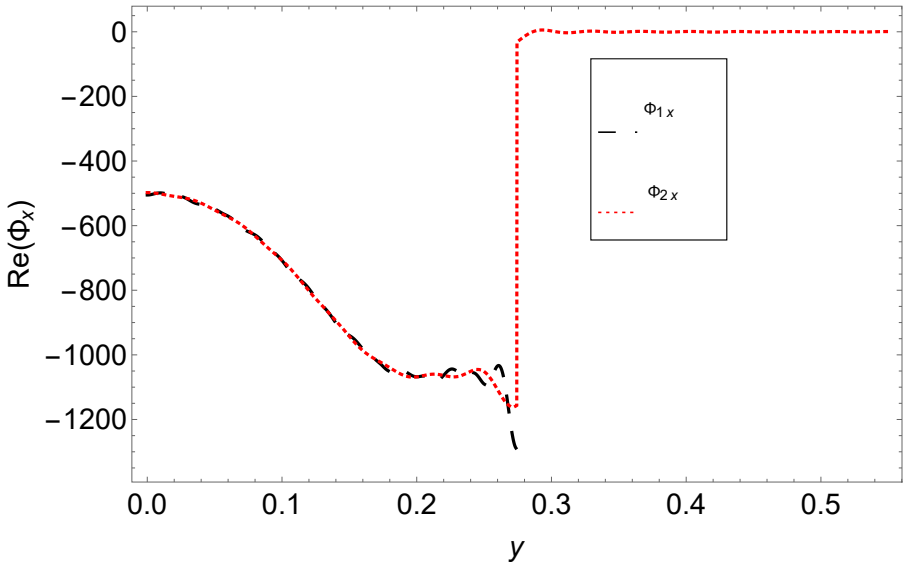

FIGURE 3.13: Real part of pressures $\Phi_1(0, y)$ and $\Phi_2(0, y)$, plotted against y, where $N = 15$ terms.

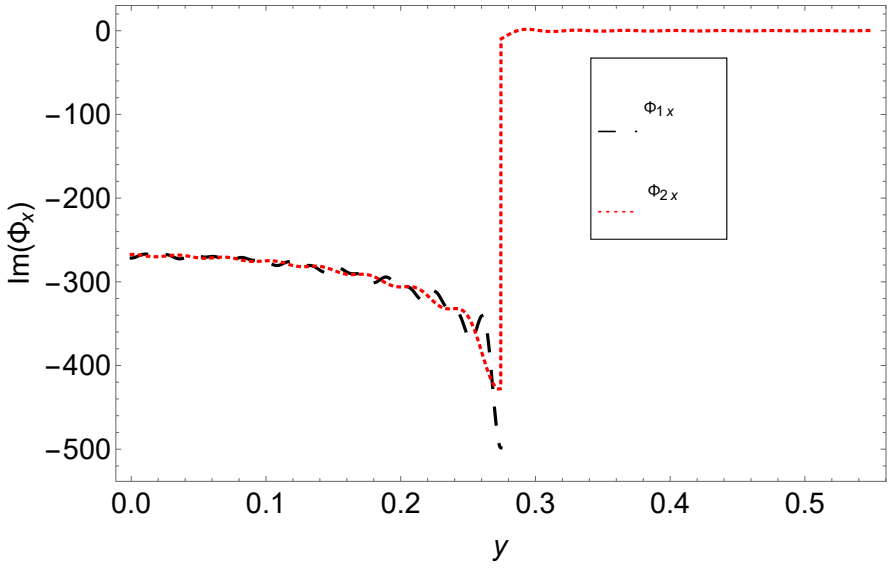

FIGURE 3.14: Real part of pressures $\Phi_1(0, y)$ and $\Phi_2(0, y)$, plotted against y, where $N = 15$ terms.

Chapter 4

Chamber-Silencer with Porous Lining

In this chapter, a physical problem involving porous material is solved by using Mode-matching technique. The problem contains four regions. The central region involves porous material. The problem is radiated with source from the inlet which is attenuated by the chamber and passes through the outlet.

4.1 Mathematical Formulation

In this problem we have four regions R_1, R_2, R_3 and R_4. The region R_1 is bounded by rigid walls and comprises sound source at $(x, y) = (a, b)$. The region R_2 contains sound absorbent material which is separated from air the air medium through a porous lining at $y = h_3$. The region R_3 has rigid boundaries at $y = h_2$ and $y = h_3$. The region R_4 has acoustically rigid boundaries at $x > L$, $y = 0$ and $y = h_1$. The sound wave is incident from region R_1 which transmitted in region R_4, while reflection is in regions R_1, R_2 and R_3. The geometry of problem is shown in Fig.1.

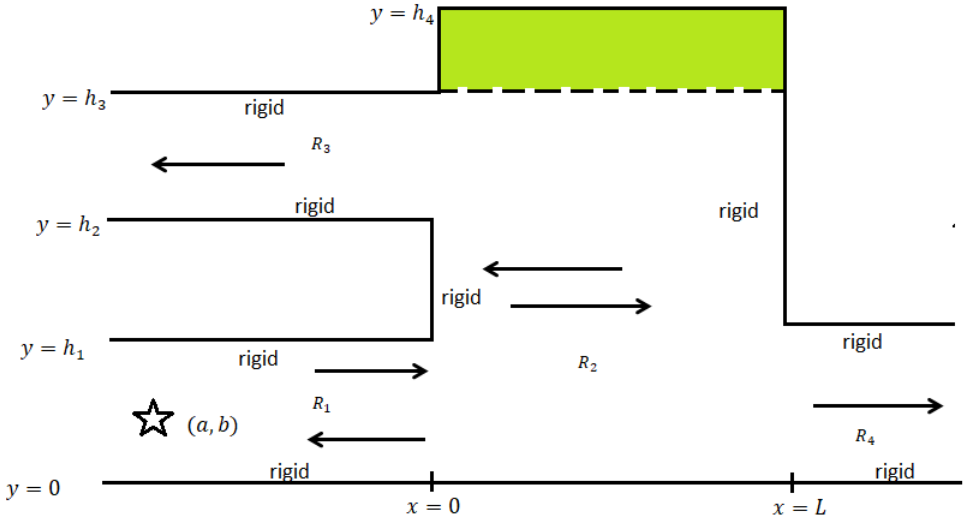

FIGURE 4.1: The geometry of the semi-infinite duct

The dimensionless fluid potential $\Phi(x, y)$ in the waveguide can be expressed as

$$\Phi(x,y) = \begin{cases} \Phi_1(x,y), & x < 0, \quad 0 \le y \le h_1, \\ \Phi_2(x,y), & x > 0, \quad 0 \le y \le h_4, \\ \Phi_3(x,y), & x < 0, \quad h_2 \le y \le h_3, \\ \Phi_4(x,y), & x > 0, \quad 0 \le y \le h_1. \end{cases} \tag{4.1}$$

The rigid boundary conditions for regions R_i, $i = 1, 2, 3, 4$ are given as

$$\frac{\partial \Phi_1(x,y)}{\partial y} = 0, \quad y = 0, \ h_1, \tag{4.2}$$

$$\frac{\partial \Phi_2(x,y)}{\partial y} = 0, \quad y = 0, \ h_4, \tag{4.3}$$

$$\frac{\partial \Phi_3(x,y)}{\partial y} = 0, \quad y = h_2, \ h_3, \tag{4.4}$$

$$\frac{\partial \Phi_4(x,y)}{\partial y} = 0, \quad y = 0, \ h_1. \tag{4.5}$$

4.2 Mode-Matching Solution

We apply Mode-matching technique to solve the boundary value problem. First we determine the eigenfunction expansion of region R_1. In this region the fluid potential $\Phi_1(x,y)$ is the sum of incident field $\Phi_1^{\mathrm{i}}(x,y)$ and reflected field $\Phi_1^{\mathrm{r}}(x,y)$

$$\Phi_1(x,y) = \Phi_1^{\mathrm{i}}(x,y) + \Phi_1^{\mathrm{r}}(x,y). \tag{4.6}$$

The governing Helmholtz's equation for region R_1 at $x = a$ and $y = b$ is

$$\left\{\frac{\partial^2}{\partial x^2} + \frac{\partial^2}{\partial y^2} + 1\right\}\Phi_1(x,y) = -J\delta(x-a)\delta(y-b), \tag{4.7}$$

while at $x \neq a$ and $y \neq b$ is

$$\left\{\frac{\partial^2}{\partial x^2} + \frac{\partial^2}{\partial y^2} + 1\right\}\Phi_1(x,y) = 0. \tag{4.8}$$

As the conditions for region R_1 are same as in previous problem, therefore $\Phi_1^{\mathrm{i}}(x,y)$ and $\Phi_1^{\mathrm{r}}(x,y)$ will be same i.e.

$$\Phi_1^{\mathrm{r}}(x,y) = \sum_{n=0}^{\infty} A_n \varphi_{1n}(y) e^{-i\eta_n x}, \tag{4.9}$$

$$\Phi_1^{\mathrm{i}}(x,y) = \sum_{n=0}^{\infty} iJ \frac{\varphi_{1n}(y)\varphi_{1n}(b)}{2\eta_n} e^{i\eta_n|x-a|}. \tag{4.10}$$

On substituting (4.9) and (4.10) into (4.6), we achieve

$$\Phi_1(x,y) = iJ\sum_{n=0}^{\infty} \frac{\varphi_{1n}(y)\varphi_{1n}(b)}{2\eta_n} e^{i\eta_n|x-a|} + \sum_{n=0}^{\infty} A_n \varphi_{1n}(y) e^{-i\eta_n x}. \tag{4.11}$$

The governing Helmholtz's equation for region R_2, for air medium is

$$\left\{\frac{\partial^2}{\partial x^2} + \frac{\partial^2}{\partial y^2} + 1\right\}\Phi_2(x,y) = 0, \quad 0 \leq y \leq h_3, \tag{4.12}$$

while for porous medium it takes form

$$\left\{\frac{\partial^2}{\partial x^2}+\frac{\partial^2}{\partial y^2}+\Gamma^2\right\}\Phi_2(x,y)=0, \quad h_3\le y\le h_4, \tag{4.13}$$

where Γ is the non-dimensional propagation constant and is

$$\Gamma=1+ia_1\xi^{a_2}+a_3\xi^{a_4}. \tag{4.14}$$

The normalized complex density in non-dimensional form is given by

$$\beta=\Gamma\left(1+a_5\xi^{a_6}-ia_7\xi^{a_8}\right). \tag{4.15}$$

Here,
$\xi=\dfrac{f\rho}{\sigma}$, is the non-dimensional parametric frequency in porous medium,
$\sigma=A_1\rho_b^{A_2}$, is the flow resistivity,

ρ_b is bulk density and f is the excitation frequency,

the constants $a_1, a_2, ..., a_8$ and $A_1 - A_2$ are determined experimentally and for different porous material their values are different.
The fluid potential in region R_2 can be expressed as eigenfunction expansion formulation given by

$$\Phi_2(x,y)=\sum_{n=0}^{\infty}\left\{B_ne^{is_nx}+C_ne^{-is_nx}\right\}Y_n(y), \tag{4.16}$$

where

$$Y_n(y)=\begin{cases}\cosh(\gamma_n y), & 0\le y\le h_3,\\ \\ -\dfrac{\gamma_n\sinh(\gamma_n h_3)\cosh\left[\lambda_n(h_4-y)\right]}{\lambda_n\sinh\left[\lambda_n(h_4-h_3)\right]}, & h_3\le y\le h_4.\end{cases} \tag{4.17}$$

The governing Helmholtz's equation for region R_3 is

$$\left\{\frac{\partial^2}{\partial x^2}+\frac{\partial^2}{\partial y^2}+1\right\}\Phi_3(x,y)=0, \quad h_2\le y\le h_3. \tag{4.18}$$

Now to solve (4.18) subject to rigid boundary condition (4.4), the eigen expansion form of reflected duct modes is assumed as,

$$\Phi_3(x,y) = \sum_{n=0}^{\infty} D_n \Phi_{3n}(x,y), \tag{4.19}$$

where $D_n, n = 0, 1, 2, ...$ are the amplitudes of reflected duct modes and $\Phi_{3n}(x,y), n = 0, 1, 2, ...$ contains shape and direction of reflected modes. To find $\Phi_{3n}(x,y)$ from boundary conditions for region R_3, we use separation of variable method. For this we assume

$$\Phi_{3n}(x,y) = X_{3n}(x)\psi_{3n}(y). \tag{4.20}$$

On using (4.20) into (4.18), we get

$$X_{3n}(x) = c_{13}e^{i\nu_n x} + c_{14}e^{-i\nu_n x} \tag{4.21}$$

and

$$\psi_{3n}(y) = c_{15}\cos(\tau_n y) + c_{16}\sin(\tau_n y), \tag{4.22}$$

where

$$\nu_n = \sqrt{1-\tau_n^2}. \tag{4.23}$$

From rigid boundary conditions (4.4), at $y = h_2$ we obtain

$$\frac{d\psi_{3n}}{dy}(h_2) = 0. \tag{4.24}$$

On using (4.22) into (4.24), we get

$$c_{16} = \frac{\sin(\tau_n h_2)}{\cos(\tau_n h_2)} c_{15},$$

which on invoking back into (4.22), yields

$$\psi_{3n}(y) = \frac{c_{15}}{\cos(\tau_n h_2)} \cos\left[\tau_n (y - h_2)\right]. \tag{4.25}$$

Now from (4.4), we can write the rigid condition at $y = h_3$ as

$$\frac{d\psi_{3n}}{dy}(h_3) = 0. \tag{4.26}$$

On using (4.25) into (4.26), we get

$$\sin\left[\tau_n(h_3 - h_2)\right] = 0, \tag{4.27}$$

which yields eigenvalues $\tau_n = \dfrac{n\pi}{h_3 - h_2}, n = 0, 1, 2, ...$ the resulting eigenfunctions $\psi_{3n}(y) = \cos\left[\tau_n(y - h_2)\right]$ are orthogonal and satisfy the orthogonality relation

$$\int_{h_2}^{h_3} \psi_{3n}\psi_{3m}dy = \frac{h_3 - h_2}{2}\epsilon_m\delta_{mn}. \tag{4.28}$$

Thus, we can write the orthonormal relation

$$\int_{h_2}^{h_3} \varphi_{3n}(y)\varphi_{3m}(y)dy = \delta_{mn}, \tag{4.29}$$

where

$$\varphi_{3m}(y) = \sqrt{\frac{2}{(h_3 - h_2)\epsilon_m}}\ \psi_{3n}(y).$$

As reflection takes place in negative x direction only, therefore $c_{13} = 0$ and reflected field in R_3 can be given by

$$\Phi_3(x, y) = \sum_{n=0}^{\infty} D_n\varphi_{3n}(y)e^{-i\nu_n x}. \tag{4.30}$$

The fluid potential $\Phi_4(x, y)$ in the region R_4 satisfies

$$\left\{\frac{\partial^2}{\partial x^2} + \frac{\partial^2}{\partial y^2} + 1\right\}\Phi_4(x, y) = 0, \quad 0 \le y \le h_1. \tag{4.31}$$

The fluid potential in this region can be find by using separation of variable method as used for $\Phi_1(x, y)$, accordingly by using the separation of variable method, that gives

$$\Phi_4(x, y) = \sum_{n=0}^{\infty} E_n\varphi_{1n}(y)e^{i\eta_n(x-L)}. \tag{4.32}$$

The modal coefficients $\{A_n, B_n, C_n, D_n, E_n\}$ are unknowns. To determine these unknowns, we apply matching conditions at $x = 0$ and $x = L$, that are

$$\Phi_1(0, y) = \Phi_2(0, y), \quad 0 \le y \le h_1, \tag{4.33}$$

$$\Phi_3(0, y) = \Phi_2(0, y), \quad h_2 \le y \le h_3, \tag{4.34}$$

$$\Phi_4(L, y) = \Phi_2(L, y), \quad 0 \le y \le h_1, \tag{4.35}$$

$$\Phi_{2x}(0, y) = \begin{cases} \Phi_{1x}(0, y), & 0 \le y \le h_1, \\ 0, & h_1 \le y \le h_2, \\ \Phi_{3x}(0, y), & h_2 \le y \le h_3, \\ 0, & h_3 \le y \le h_4, \end{cases} \tag{4.36}$$

$$\Phi_{2x}(L, y) = \begin{cases} \Phi_{4x}(L, y), & 0 \le y \le h_1, \\ 0, & h_1 \le y \le h_4. \end{cases} \tag{4.37}$$

By using (4.11) and (4.16) into (4.33), we find

$$iJ \sum_{n=0}^{\infty} \frac{\varphi_{1n}(y)\varphi_{1n}(b)}{2\eta_n} e^{i\eta_n|-a|} + \sum_{n=0}^{\infty} A_n \varphi_{1n}(y) = \sum_{n=0}^{\infty} \{B_n + C_n\} Y_n(y). \tag{4.38}$$

Multiplying with $\varphi_{1m}(y)$ and integrating over $0 \le y \le h_1$

$$\begin{aligned} iJ \sum_{n=0}^{\infty} \int_0^{h_1} \frac{\varphi_{1n}(y)\varphi_{1n}(b)}{2\eta_n} e^{i\eta_n|-a|} \varphi_{1m}(y) dy + \sum_{n=0}^{\infty} A_n \int_0^{h_1} \varphi_{1n}(y)\varphi_{1m}(y) dy \\ = \sum_{n=0}^{\infty} \{B_n + C_n\} \int_0^{h_1} \varphi_{1m}(y) Y_n(y) dy. \end{aligned} \tag{4.39}$$

On using orthogonality relation (3.23), we get

$$iJ \sum_{n=0}^{\infty} \frac{\varphi_{1n}(b)}{2\eta_n} e^{i\eta_n|-a|} \delta_{mn} + \sum_{n=0}^{\infty} A_n \delta_{mn} = \sum_{n=0}^{\infty} \{B_n + C_n\} \int_0^{h_1} \varphi_{1m}(y) Y_n(y) dy, \tag{4.40}$$

or

$$Q_m^i + A_m = \sum_{n=0}^{\infty} \{B_n + C_n\} R_{mn}, \tag{4.41}$$

where

$$R_{mn} = \int_0^{h_1} \varphi_{1m}(y) Y_n(y) dy \tag{4.42}$$

and

$$Q_m^i = iJ \frac{\varphi_{1m}(b)}{2\eta_m} e^{i\eta_m|-a|}. \tag{4.43}$$

Likewise on using (4.16) and (4.30) into (4.34) gives

$$\sum_{n=0}^{\infty} D_n \varphi_{3n}(y) = \sum_{n=0}^{\infty} \{B_n + C_n\} Y_n(y). \tag{4.44}$$

Multiplying with $\varphi_{3m}(y)$ and integrating over $h_2 \leq y \leq h_3$,

$$\sum_{n=0}^{\infty} D_n \int_{h_2}^{h_3} \varphi_{3m}(y) \varphi_{3n}(y) dy = \sum_{n=0}^{\infty} \{B_n + C_n\} \int_{h_2}^{h_3} Y_n(y) \varphi_{3m}(y) dy. \tag{4.45}$$

By using orthonormal relation (4.29), we obtain

$$D_m = \sum_{n=0}^{\infty} \{B_n + C_n\} P_{mn}, \tag{4.46}$$

where

$$P_{mn} = \int_{h_2}^{h_3} Y_n(y) \varphi_{3m}(y) dy. \tag{4.47}$$

Accordingly, we substitute (4.16) and (4.32) into (4.35) to achieve

$$\sum_{n=0}^{\infty} E_n \varphi_{1n}(y) = \sum_{n=0}^{\infty} \left\{B_n e^{is_n L} + C_n e^{-is_n L}\right\} Y_n(y). \tag{4.48}$$

On multiplying (4.48) with $\varphi_{1m}(y)$, integrating over $0 \leq y \leq h_1$, we get

$$\sum_{n=0}^{\infty} E_n \int_0^{h_1} \varphi_{1n}(y) \varphi_{1m}(y) dy = \sum_{n=0}^{\infty} \left\{B_n e^{is_n L} + C_n e^{-is_n L}\right\} \int_0^{h_1} \varphi_{1m}(y) Y_n(y) dy. \tag{4.49}$$

On using orthogonality relation (3.23), we obtain

$$E_m = \sum_{n=0}^{\infty} \left\{ B_n e^{is_n L} + C_n e^{-is_n L} \right\} R_{mn}, \tag{4.50}$$

Now to incorporate velocity conditions, we substitute (4.11), (4.16) and (4.30) into (4.36), we find

$$i \sum_{n=0}^{\infty} \{B_n - C_n\} s_n Y_n(y) = \begin{cases} J \sum_{n=0}^{\infty} \dfrac{\varphi_{1n}(y)\varphi_{1n}(b)}{2} e^{i\eta_n|-a|} \dfrac{a}{|a|} - \sum_{n=0}^{\infty} A_n \varphi_{1n}(y)\eta_n, & \\ & 0 \le y \le h_1, \\ 0, & h_1 \le y \le h_2, \\ -i \sum_{n=0}^{\infty} D_n \nu_n \varphi_{3n}(y), & h_2 \le y \le h_3, \\ 0 & h_3 \le y \le h_4. \end{cases} \tag{4.51}$$

On multiplying with $Y_{1m}(y)$, integrating over $0 \le y \le h_3$

$$\begin{aligned} i \sum_{n=0}^{\infty} \{B_n - C_n\} s_n \int_0^{h_3} Y_{1n} Y_{1m} dy = J \sum_{n=0}^{\infty} \frac{\varphi_{1n}(b)}{2} e^{i\eta_n|-a|} \frac{a}{|a|} \int_0^{h_1} \varphi_{1n}(y) Y_{1m}(y) dy \\ -i \sum_{n=0}^{\infty} \eta_n \int_0^{h_1} \varphi_{1n}(y) Y_{1m}(y) dy - i \sum_{n=0}^{\infty} D_n \nu_n \int_{h_2}^{h_3} \varphi_{3n}(y) Y_{1m}(y) dy. \end{aligned} \tag{4.52}$$

or

$$i \sum_{n=0}^{\infty} \{B_n - C_n\} s_n \int_0^{h_3} Y_{1n} Y_{1m} dy = F_m^i - i \sum_{n=0}^{\infty} A_n \eta_n R_{nm} - i \sum_{n=0}^{\infty} D_n \nu_n P_{nm}, \tag{4.53}$$

where

$$F_m^i = J \frac{\varphi_{1m}(b)}{2} e^{i\eta_m|-a|} \frac{a}{|a|} \int_0^{h_1} \varphi_{1m}(y) Y_{1m}(y) dy. \tag{4.54}$$

On multiplying (4.51) by $Y_{2m}(y)$, integrating over $h_3 \le y \le h_4$, we find

$$i \sum_{n=0}^{\infty} \{B_n - C_n\} s_n \int_{h_3}^{h_4} Y_{2n} Y_{2m} dy = 0. \tag{4.55}$$

Now multiply (4.55) with β and add into (4.53) to obtain

$$\begin{aligned} i\sum_{n=0}^{\infty}\{B_n - C_n\}\, s_n \left[\int_0^{h_3} Y_{1n}Y_{1m}dy + \beta\int_{h_3}^{h_4} Y_{2n}Y_{2m}dy\right] \\ = F_m^i - i\sum_{n=0}^{\infty} A_n\eta_n R_{nm} - i\sum_{n=0}^{\infty} D_n\nu_n P_{nm}. \end{aligned} \tag{4.56}$$

On using orthogonality relation (3.98), (4.56) leads to

$$i\sum_{n=0}^{\infty}\{B_n - C_n\}\, s_n\delta_{mn}G_n = F_m^i - i\sum_{n=0}^{\infty} A_n\eta_n R_{nm} - i\sum_{n=0}^{\infty} D_n\nu_n P_{nm} \tag{4.57}$$

or

$$B_m - C_m = \frac{1}{is_mG_m}\left[F_m^i - i\sum_{n=0}^{\infty} A_n\eta_n R_{nm} - i\sum_{n=0}^{\infty} D_n\nu_n P_{nm}\right]. \tag{4.58}$$

Now on substituting (4.16) and (4.32) into (4.37), we get

$$\sum_{n=0}^{\infty} is_n\left(B_ne^{is_nL} - C_ne^{-is_nL}\right)Y_n(y) = \begin{cases} \sum_{n=0}^{\infty} E_ni\eta_n\varphi_{1n}(y), & 0 \le y \le h_1, \\ 0, & h_1 \le y \le h_4. \end{cases} \tag{4.59}$$

Multiplying (4.59) by $Y_m(y)$ and integrating over $0 \le y \le h_4$, we obtain

$$\sum_{n=0}^{\infty} is_n\left(B_ne^{is_nL} - C_ne^{-is_nL}\right)\int_0^{h_4} Y_n(y)Y_m(y)dy = \sum_{n=0}^{\infty} E_ni\eta_n\int_0^{h_1}\varphi_{1n}(y)Y_m(y)dy, \tag{4.60}$$

or

$$B_me^{is_mL} - C_me^{-is_mL} = \frac{1}{s_mG_m}\sum_{n=0}^{\infty} E_n\eta_n R_{nm}. \tag{4.61}$$

By fixing $m = n = 0, 1, 2, ...N$, we get $5(N+1)$ number of equations with $5(N+1)$ unknowns. These are solved simultaneously to get these unknowns.

4.3 Energy Flux

The energy flux/power in closed region can be defined as [69]

$$\text{Energy flux} = \frac{1}{2}\Re\left[i\int_{\Omega}\Phi(\frac{\partial\Phi}{\partial x})^{*}d\Omega\right], \tag{4.62}$$

where Ω is the domain of region. The transmission loss is defined by [70]

$$TL = -20\log\left[\frac{P_t}{P_i}\right]. \tag{4.63}$$

The incident and reflected power can be calculated by using (4.11) into (4.62),

$$\begin{aligned}\text{Energy flux}|_{R_1} = \frac{1}{2}\Re\sum_{n=0}^{\infty}\sum_{m=0}^{\infty}\Bigg[&-i|J|^2\frac{\varphi_{1n}(b)\varphi_{1m}(b)}{4\eta_n}e^{i|x-a|(\eta_n-\eta_m^*)}\frac{x-a}{|x-a|}\\ &+\frac{J\varphi_{1n}(b)A_m^*\eta_m^*}{2\eta_n}e^{i\eta_n|x-a|}e^{i\eta_m^*x}-\frac{iJ^*A_n\varphi_{1m}(b)}{2}e^{-i\eta_m^*|x-a|}e^{-i\eta_n x}\frac{x-a}{|x-a|}\\ &-A_nA_m^*e^{ix(\eta_m^*-\eta_n)}\Bigg]\int_0^{h_1}\varphi_{1n}(y)\varphi_{1m}(y)dy.\end{aligned} \tag{4.64}$$

On using orthogonality relation (3.23) into (4.64), we achieved

$$\begin{aligned}\text{Energy flux}|_{R_1} = \frac{1}{2}\Re\sum_{m=0}^{\infty}\left[|J|^2\frac{|\varphi_{1m}(b)|^2}{4\eta_m}e^{i|x-a|(\eta_m-\eta_m^*)}\frac{x-a}{|x-a|}\right]-\\ \frac{1}{2}\Re\sum_{m=0}^{\infty}\Bigg[A_m|^2\eta_m^{\star}e^{-ix(\eta_m-\eta_m^*)}+J\frac{\varphi_{1m}(b)}{2\eta_m}e^{i\eta_m|x-a|}e^{i\eta_m^*x}A_m^*\eta_m^*+\\ iJ^*\varphi_{1m}(b)A_me^{-i\eta_m x}e^{-i\eta_m^*|x-a|}\frac{x-a}{|x-a|}\Bigg].\end{aligned} \tag{4.65}$$

From (4.65) we can write the incident power as

$$P_i = \frac{1}{2}\Re\left[|J|^2\frac{|\varphi_{1m}(b)|^2}{4\eta_m}e^{i|x-a|(\eta_m-\eta_m^*)}\frac{x-a}{|x-a|}\right]. \tag{4.66}$$

Likewise, the reflected power can be written from (4.65)

$$P_r = \frac{1}{2}\Re\sum_{m=0}^{\infty}\left[A_m|^2\eta_m^{\star}e^{-ix(\eta_m-\eta_m^*)} + J\frac{\varphi_{1m}(b)}{2\eta_m}e^{i\eta_m|x-a|}e^{i\eta_m^*x}A_m^*\eta_m^* + iJ^*\varphi_{1m}(b)A_m e^{-i\eta_m x}e^{-i\eta_m^*|x-a|}\frac{x-a}{|x-a|}\right]. \quad (4.67)$$

Now to find transmitted power in 4^{th} region, we substitute (4.32) into (4.62) to get

$$P_t = \frac{1}{2}\Re\left[\sum_{n=0}^{\infty}|E_n|^2\eta_n\right]. \quad (4.68)$$

On using (4.66) and (4.68) into (4.63), we obtain

$$TL = -20\log\left[\sum_{n=0}^{\infty}\frac{4|E_n|^2\eta_n^2|x-a|}{|J|^2|\varphi_{1n}(b)|^2(x-a)e^{i|x-a|(\eta_n-\eta_n^*)}}\right]. \quad (4.69)$$

4.4 Numerical Results

In this section, the infinite linear algebraic equations defined in (4.41), (4.46), (4.50), (4.57) and (4.61) are truncated upto $n = 0, 1, 2, ..., N$ terms and then the retained system is solved numerically. The reduced system contains $5(N+1)$ equations. By solving these equations, we obtain the coefficients $A_n, B_n, C_n, D_n, E_n, n = 0, 1, 2, ..., N$. Once these coefficients are known the pressures and velocities can be plotted at interface. In order to show the graphs on fixing the duct heights at $h_1 = 0.06m$, $h_2 = 0.085m$, $h_3 = 0.1m$ and $h_4 = 0.15m$, $L = 0.05m$, the pressures and normal velocities components are plotted against non-dimensional duct heights at interface in Figs. 4.2-4.11. The physical parameters chosen are, $c = 343.5ms^{-1}$ and $\rho = 1.2043kgm^{-1}$, $a_1 = 0.2202$, $a_2 = -0.5850$, $a_3 = 0.2010$, $a_4 = -0.5829$, $a_5 = 0.0954$, $a_6 = -0.6687$, $a_7 = 0.1689$, $a_8 = -0.5707$, $A_1 = 5.774$, $A_2 = 1.792$. Note that the source is placed at $a = -0.2m$ and $b = 0.03m$ with strength $J = 500$.

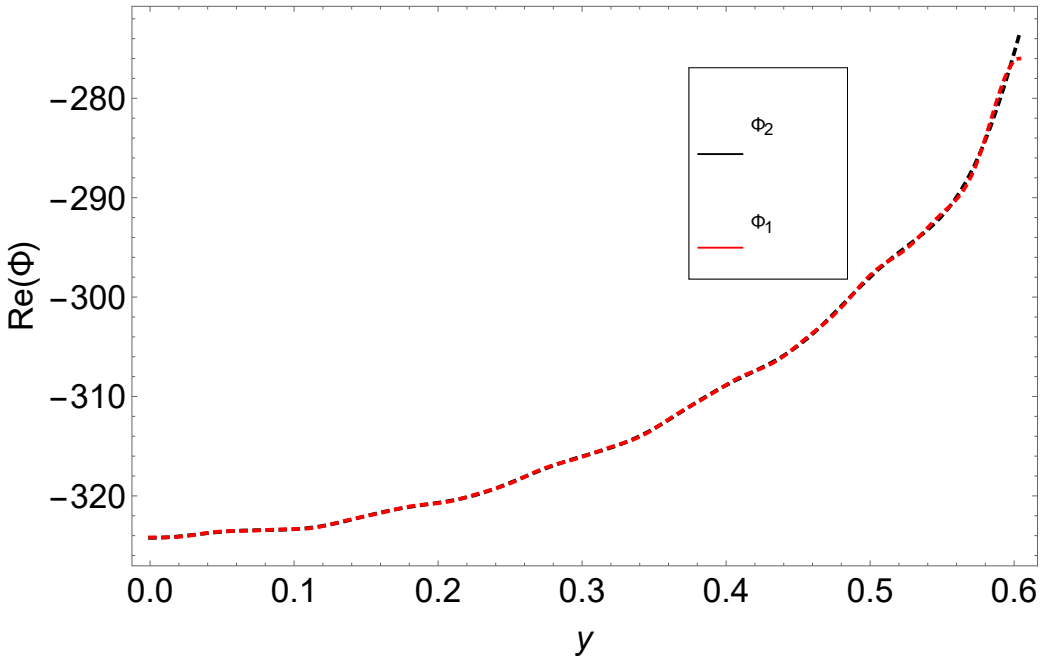

FIGURE 4.2: Real part of pressures $\Phi_1(0, y)$ and $\Phi_2(0, y)$, plotted against y, where $N = 8$ terms.

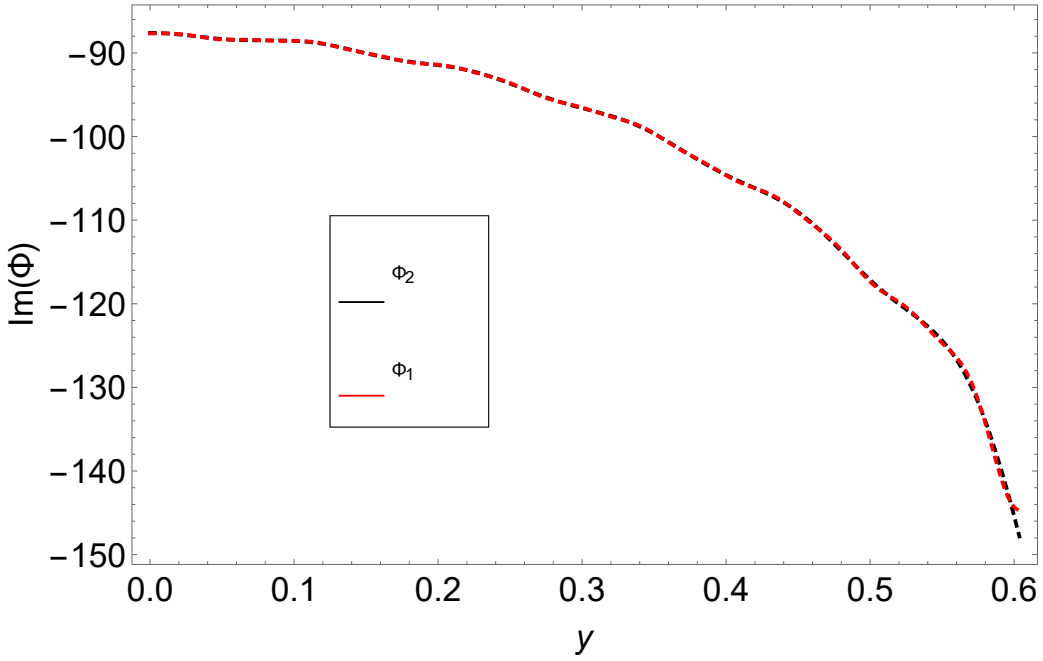

FIGURE 4.3: Imaginary part of pressures $\Phi_1(0, y)$ and $\Phi_2(0, y)$, plotted against y, where $N = 8$ terms.

Figs. 4.2 and 4.3 show the real and imaginary parts of pressures $\Phi_1(0, y)$ and $\Phi_2(0, y)$ in the regions $0 \leq y \leq h_1$. From figures we can see that pressures in fluid regions coincide. It shows that the truncated terms of solution satisfy the matching conditions.

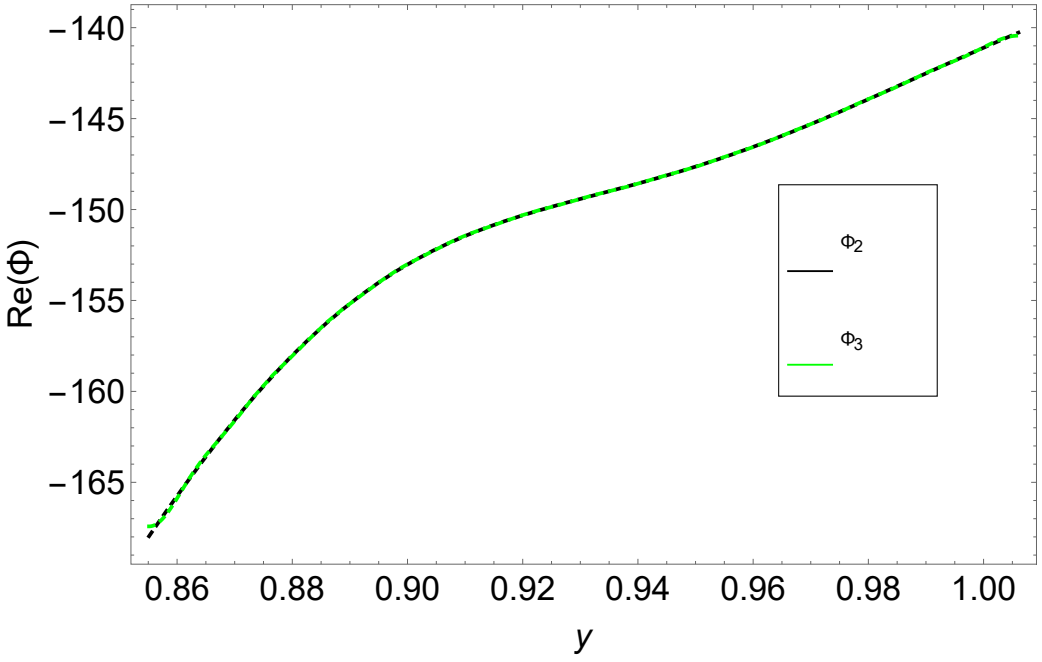

FIGURE 4.4: Real part of pressures $\Phi_2(0, y)$ and $\Phi_3(0, y)$, plotted against y, where $N = 8$ terms.

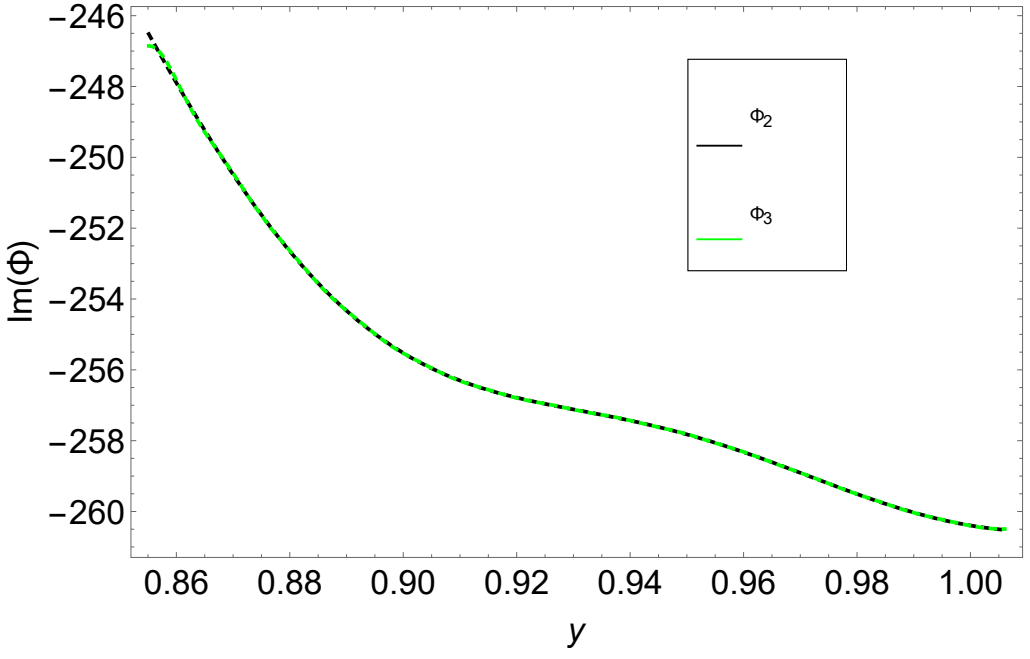

FIGURE 4.5: Imaginary part of pressures $\Phi_2(0, y)$ and $\Phi_3(0, y)$, plotted against y, where $N = 8$ terms.

Figs. 4.4 and 4.5 show the real and imaginary parts of pressures $\Phi_2(0, y)$ and $\Phi_3(0, y)$ in the regions $h_2 \leq y \leq h_3$. Also Figs. 4.6 and 4.7 show the real and imaginary parts of pressures $\Phi_2(L, y)$ and $\Phi_4(L, y)$ in the regions $0 \leq y \leq h_1$. It can be observed from figures that the pressures in fluid regions agree very well. That gives the truncated terms of solution satisfy the matching conditions.

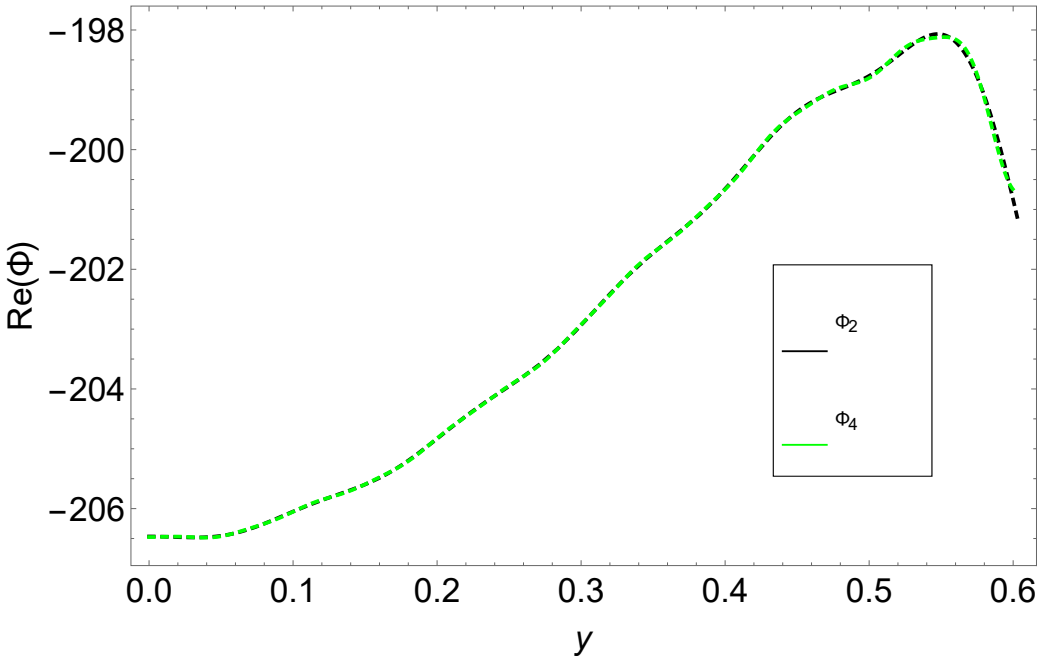

FIGURE 4.6: Real part of pressures $\Phi_2(L, y)$ and $\Phi_4(L, y)$, plotted against y, where $N = 8$ terms.

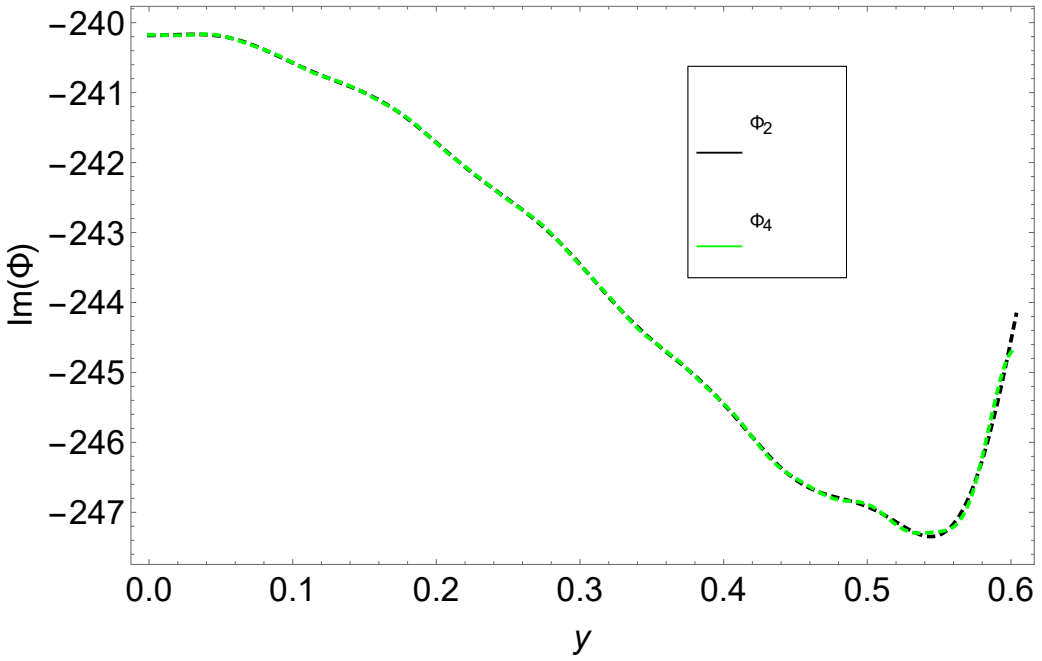

FIGURE 4.7: Imaginary part of pressures $\Phi_2(L, y)$ and $\Phi_4(L, y)$, plotted against y, where $N = 8$ terms.

Likewise, Figs. 4.8 and 4.9 show the real and imaginary parts of velocities $\Phi_{1x}(0,y)$, $\Phi_{2x}(0,y)$ and $\Phi_{3x}(0,y)$ in the regions $0 \leq y \leq h_1$, $0 \leq y \leq h_4$ and $h_2 \leq y \leq h_3$, respectively. From figures we can see that the velocities in fluid regions agree very well.

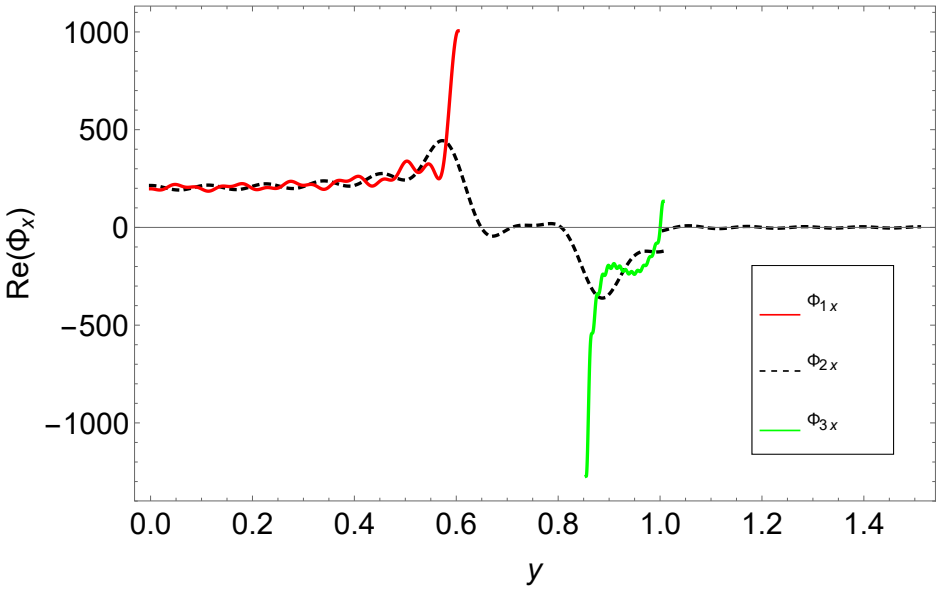

FIGURE 4.8: Real part of velocities $\Phi_{1x}(0,y)$, $\Phi_{2x}(0,y)$ and $\Phi_{3x}(0,y)$, plotted against y, where $N = 8$ terms.

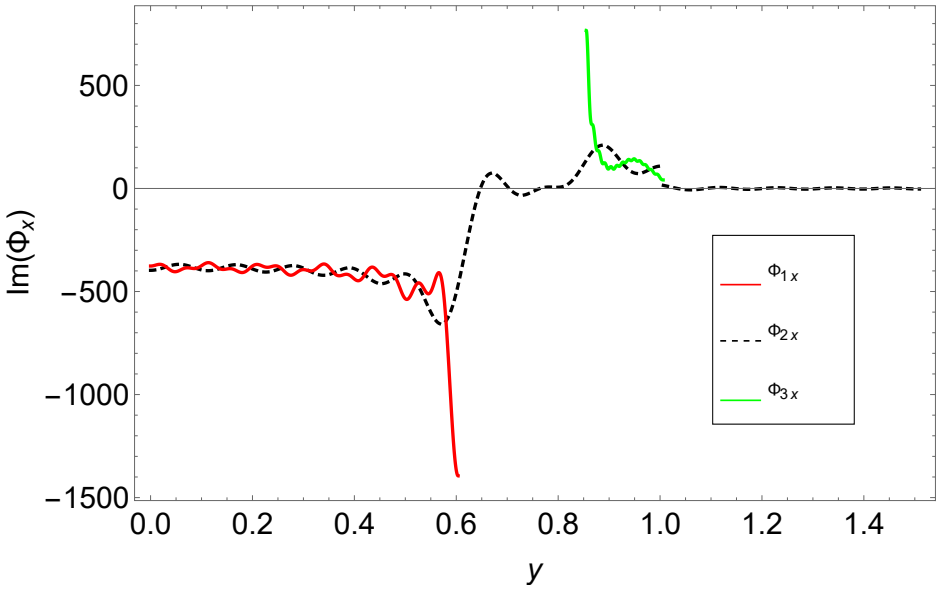

FIGURE 4.9: Imaginary part of velocities $\Phi_{1x}(0,y)$, $\Phi_{2x}(0,y)$ $\Phi_{3x}(0,y)$, plotted against y, where $N = 8$ terms.

Figs. 4.10 and 4.11 show the real and imaginary parts of velocities $\Phi_{2x}(L, y)$ and $\Phi_{4x}(L, y)$ in the interval $0 \leq y \leq h_1$. It can be observed from figures that the velocities coincide. It shows that the truncated terms of solution satisfy the matching conditions.

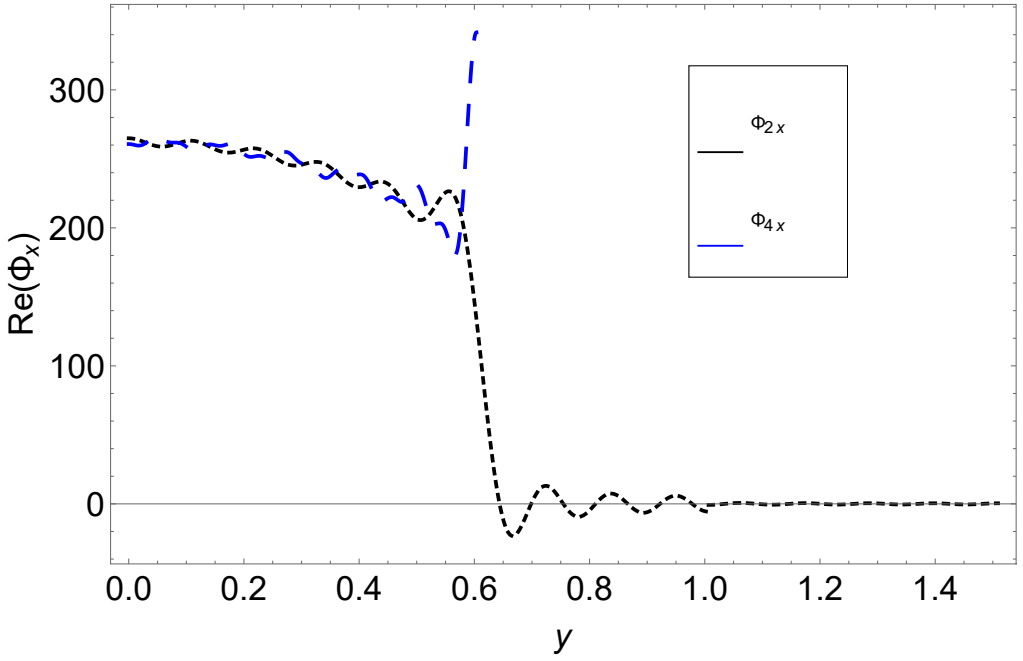

FIGURE 4.10: Real part of Velocities $\Phi_{2x}(L, y)$ and $\Phi_{4x}(L, y)$, plotted against y, where $N = 8$ terms.

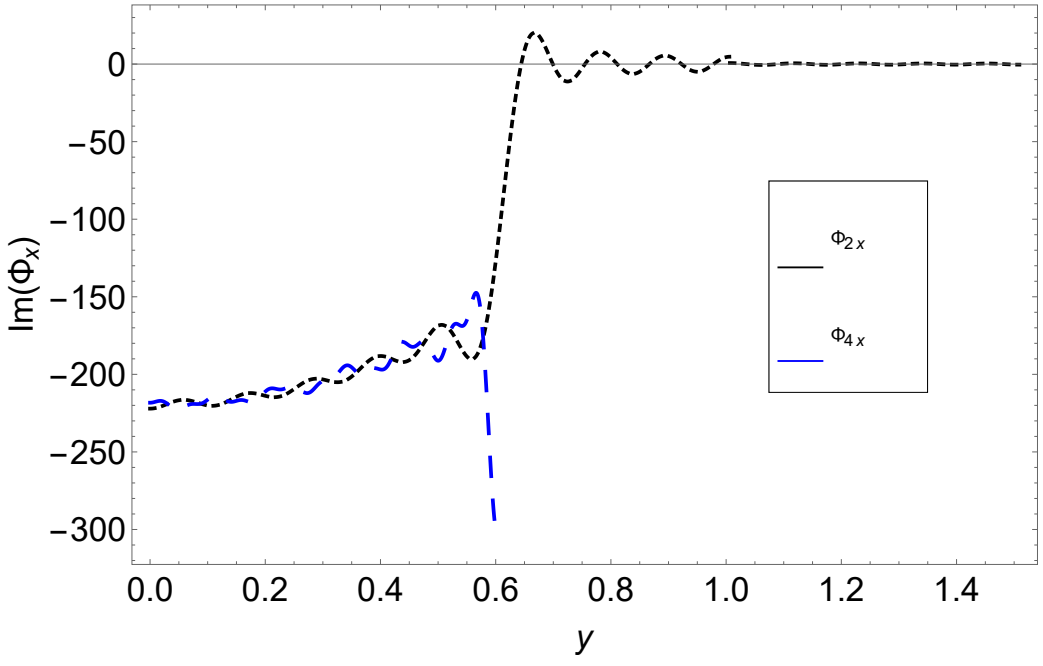

FIGURE 4.11: Imaginary part of velocities $\Phi_{2x}(L, y)$ and $\Phi_{4x}(L, y)$, plotted against y, where $N = 8$ terms.

Now we will show the graphs of transmission loss with the physical parameters are taken as $h_1 = 0.06$, $h_2 = 0.085$, $h_3 = 0.1$, $h_4 = 0.13$ and $L = 0.03$.

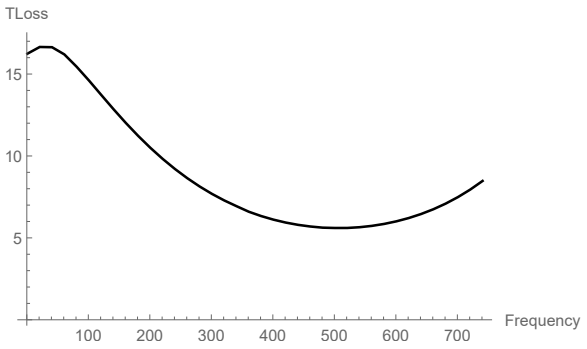

FIGURE 4.12: Transmission loss against frequency for rigid walls with porous medium.

From Fig. 4.12 it can be seen that by increasing the length L of the Chamber the transmission loss is increased.

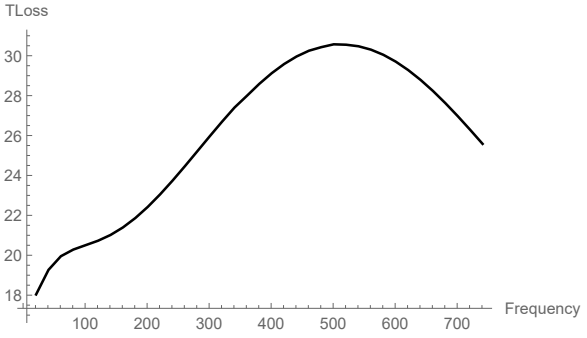

FIGURE 4.13: Transmission loss against frequency for rigid walls with porous medium with $L = 0.1$.

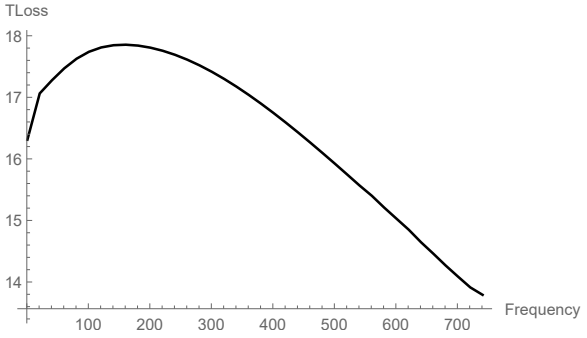

FIGURE 4.14: Transmission loss against frequency for rigid walls with porous medium with $L = 0.05$, $h_1 = 0.05$, $h_2 = 0.1$, $h_3 = 0.15$ and $h_4 = 0.5$.

From Fig. 4.14 it can be observed that by increasing the length of porous medium the transmission loss is increased.

Chapter 5

Conclusion

The Chapter wise summary and conclusion of the present study are enclosed in this Chapter. Chapter 1 depicts background and literature survey relevant to the current study along with thesis structure. In Chapter 2 useful definitions and some derivations are included. Chapter 3 consists of two problems with numerical results. In first problem we have discussed two regions with step discontinuity along with a source in the first region. Mode-matching technique is used to solve the governing system. The matching conditions of pressures and velocities are satisfied. The incidence, reflection and transmission of energy is shown graphically. The sum of reflected and transmitted power is equal to incident power and which have been shown graphically. The second non-dimensional problem consists of a porous region. The second problem is also solved with Mode-matching technique and the matching conditions confirms the accuracy of truncated solution. In chapter 4 we have discussed a problem with four regions. In the first region sound source is located. The second region can be regarded as expansion chamber having porous medium. The transmission takes place in the 4^{th} region while reflection is in other regions. Numerical results have been discussed and matching conditions of pressures and velocities agree very well, which means that the truncated solution satisfy. The incident, reflected and transmitted powers for corresponding regions have been discussed. The attenuation of source radiation with expansion chamber having porous medium is investigated. It is seen that dimensions of the

chamber effect the attenuation of source radiation. The transmission is increased by increasing the length of duct.

Bibliography

[1] K. Peat, The acoustical impedance at the junction of an extended inlet or outlet duct, Journal of sound and vibration, 150(1): 101-110 (1991).

[2] M. U. Hassan and A. D. Rawlins, Sound radiation in a planar trifurcated lined duct, Wave Motion, 29(2): 157-174 (1999) .

[3] A. D. Rawlins, Radiation of sound from an unflanged rigid cylindrical duct with an acoustically absorbing internal surface, Proceedings of the Royal Society of London. A. Mathematical and Physical Sciences, 361 (1704): 65-91(1978).

[4] A. D. Rawlins, Wave propagation in a bifurcated impedance-lined cylindrical waveguide, Journal of Engineering Mathematics, 59(40): 419-435 (2007).

[5] M. Ayub, M. Ramzan, and A. Mann, Acoustic diffraction by an oscillating strip, Applied Mathematics and Computation, 214(1): 201-209 (2009).

[6] M. Ayub, M. Tiwana, and A. Mann, Acoustic diffraction in a trifurcated waveguide with mean flow, Communications in Nonlinear Science and Nu-merical Simulation, 15(12): 3939-3949(2010).

[7] M. Ayub, M. Ramzan, and A. Mann, Line source and point source diffraction by a reactive step, Journal of Modern Optics,56(7): 893-902 (2009).

[8] J. B. Lawrie and M. Afzal, Acoustic scattering in a waveguide with a height discontinuity bridged by a membrane: a tailored galerekin approach, Journal of Engineering Mathematics, 105(1): 99-115 (2017).

[9] M. Ayub, R. Nawaz and A. Naeem, Diffraction of sound waves by a finite barrier in a moving fluid, Journal of mathematical analysis and applications, 349(1): 245-258 (2009).

[10] L. Huang, Modal analysis of a drum like silencer, the Journal of the Acoustical Society of America, 112(5): 2014-2025 (2002).

[11] L. Huang, Parametric study of a drum-like silencer, Journal of sound and vibration, 269(3-5): 467-488 (2004).

[12] L. Huang, Broadband sound reflection by plates covering side-branch cavities in a duct, the Journal of the Acoustical Society of America, 119(5): 2628-2638 (2006).

[13] A. Cummings and I.J. Chang, Sound attenuation of a finite length dissipative flow duct silencer with internal mean flow in the absorbent, Journal of Sound and Vibration, 127(1): 1-17 (1988).

[14] K. S. Peat, A transfer matrix for an absorption silencer element, Journal of Sound and Vibration, 146(2): 353-360 (1991).

[15] R. Kirby, Simplified techniques for predicting the transmission loss of a circular dissipative silencer, Journal of Sound and Vibration, 243(3): 403-426 (2001).

[16] R. Folk, A. Herczynski, Solutions of elastodynamic slab problems using a new orthogonality condition, The Journal of the Acoustical Society of America, 80(4): 1103-1110 (1986).

[17] R. Folk, A. Herczynski, Orthogonality condition for the Pochhammer-Chree modes, The Quarterly Journal of Mechanics and Applied Mathematics, 42(4): 523-536 (1989).

[18] J. B. Lawrie and R. Kirby, Mode-matching without root-finding: Application to a dissipative silencer, The Journal of the Acoustical Society of America, 119(4): 2050-2061 (2006).

[19] J. B. Lawrie and R. Kirby, On analysing the performance of a dissipative silencer: a mode-matching approach, IUTAM Symposium on Asymptotics, Singularities and Homogenisation in Problems of Mechanics, 169-178 (2003).

[20] K. S. Peat and K. L. Rathi, A finite element analysis of the convected acoustic wave motion in dissipative silencers, Journal of Sound and Vibration, 184(3): 529-545 (1995).

[21] A. F. Seybert, R. A. Seman and M. D. Lattuca, Boundary element prediction of sound propagation in ducts containing bulk absorbing materials, 976-981 (1998).

[22] R. A. Scott, The propagation of sound between walls of porous material, Proceedings of the Physical Society (1926-1948), 58(4): 358 (1946).

[23] A. Bokor, Attenuation of sound in lined ducts, Journal of Sound and Vibration, 10(3): 390-403 (1969).

[24] C. Wassilieff, Experimental verification of duct attenuation models with bulk reacting linings, Journal of sound and vibration, 114(2): 239-251 (1987).

[25] R. J. Astley and A. Cummings, A finite element scheme for attenuation in ducts lined with porous material: comparison with experiment, Journal of Sound and Vibration, 116(2): 239-263 (1987).

[26] J. U. Kurze and I. L. Ver, Sound attenuation in ducts lined with non-isotropic material, Journal of Sound and Vibration, 24(2): 177-187 (1972).

[27] A. Cummings, Sound attenuation in ducts lined on two opposite walls with porous material, with some applications to splitters, Journal of Sound and Vibration, 49(1): 9-35 (1976).

[28] A. Cummings, Sound attenuation in ducts lined on two opposite walls with porous material with some application to splitters, Journal of Sound and Vibration, 49: 9-35 (1976).

[29] R. J. Astley and A. Cummings, A
finite element scheme for attenuation in ducts lined with porous material comparison with experiment, Journal of Sound and Vibration, 116: 239-263 (1987).

[30] R. Kirby and J. B. Lawrie, A point collocation approach to modelling large dissipative silencers, Journal of Sound and Vibration, 286: 313-339 (2005).

[31] R. Nawaz and J. B. Lawrie, Scattering of a fluid-structure coupled wave at a flanged junction between two flexible waveguides, The Journal of the Acoustical Society of America, 134(3): 1939-1949 (2013).

[32] R. Nawaz, M. Afzal and M. Ayub, Acoustic propagation in two-dimensional waveguide for membrane bounded ducts, Communications in Nonlinear Science and Numerical Simulation, 20(2): 421-433 (2015).

[33] M. Afzal, R. Nawaz and A. Ullah, Attenuation of dissipative device involving coupled wave scattering and change in material properties, Applied Mathematics and Computation, 290: 154-163 (2016).

[34] T. Nawaz, M. Afzal and A.Wahab, Scattering analysis of a flexible trifurcated lined waveguide structure with step-discontinuities, Physica Scripta, 96(11): 115004 (2021).

[35]] M. Afzal, T. Nawaz and R. Nawaz, Scattering characteristics of planar trifurcated waveguide structure containing multiple discontinuities, Waves in Random and Complex Media, 1-20 (2020).

[36] M. Afzal, S. Shafique and A. Wahab, Analysis of traveling waveform of flexible waveguides containing absorbent material along flanged junctions, Communication in Non-Linear Science and Numerical Simulation, 97: 105737 (2021).

[37] M. Afzal and S. Shafique, Attenuation analysis of flexural modes with absorbent lined flanges and different edge conditions, Journal of the Acoustical Society of America, 148: 85 (2020).

[38] S. Shafique, M. Afzal and R. Nawaz, On the attenuation of fluid-structure coupled modes in a non-planar waveguide, Mathematics and Mechanics of Solids, 25(10): 1-20 (2020).

[39] M. Afzal, J. U. Satti and R. Nawaz, Scattering characteristics of non-planar trifurcated waveguides, Meccanica, 55: 977-988 (2020).

[40] T. Nawaz, M. Afzal and R. Nawaz, The scattering analysis of trifurcated waveguide involving structural discontinuities, Advances in Mechanical Engineering, 11(7): 1-11 (2019).

[41] H. Bilal and M. Afzal, Acoustic wave scattering from a wave-bearing cavity in a rectangular waveguide, Journal of the Acoustical Society of America, 144: 1681 (2018).

[42] A. Ullah, R. Nawaz and M. Afzal, Fluid-structure coupled wave scattering in a flexible duct at the junction of planar discontinuities, Advances in Mechanical Engineering, 9(7): 1-11 (2017).

[43] S. Shafique, M. Afzal and R. Nawaz, On mode matching analysis of fluid-structure coupled wave scattering between two flexible waveguides, Canadian Journal of Physics, 95(6): 581-589 (2017).

[44] J. B. Lawrie and M. Afzal, Acoustic scattering in a waveguide with a height discontinuity bridged by a membrane: a tailored Galerkin approach, Journal of Engineering Mathematics, 105(1): 99-115 (2017).

[45] J. U. Satti, M. Afzal and R. Nawaz, Scattering analysis of a partitioned wave-bearing cavity containing different material properties, Physica Scripta, 94(11): 115-223 (2019).

[46] M. Afzal, R. Nawaz, M. Ayub and A. Wahab, Acoustic scattering in flexible waveguide involving step discontinuity, PloS one, 9(8): e103807 (2014).

[47] M. Afzal and J. U. Satti, The traveling wave formulation of a splitting chamber containing reactive components, Archive of Applied Mechanics, 91(5): 1959-1980 (2021).

[48] M. Ayub, R. Nawaz and A. Naeem, Diffraction of sound waves by a finite barriers in a moving fluid, Journal of Mathematical Analysis and Applications, 349(1): 245-258 (2009).

[49] M. Ayub, R. Nawaz and A. Naeem, Line source diffraction by a slit in a moving fluid, Canadian Journal of Physics, 87(11): 1139-1149 (2009).

[50] M. Ayub, R. Nawaz and A. Naeem, Diffraction of an impulsive line source with wake, Physica Scripta, 82(4): 045402 (2010).

[51] M. Ayub, A. Naeem and R. Nawaz, Sound due to an impulsive line source, Computer and Mathematics with Applications, 60(12): 3123-3129 (2010).

[52] R. Nawaz, A note on acoustic diffraction by an absorbing finite strip, Indian Journal of Pure and Applied Mathematics, 43(6): 571-589 (2012).

[53] R. Nawaz and M. Ayub, An exact and asymptotic analysis of a diffraction problem, Meccanics, 48(3): 653-662 (2013).

[54] R. Nawaz and M. Ayub, Closed form solution of electromagnetic wave diffraction problem in a homogeneous bi-isotropic medium, Mathematical Methods in the Applied Science, 38: 176-187 (2014).

[55] R. Nawaz, A. Naeem and M. Ayub, Point source diffraction by a slit in a moving fluid, Waves in Random and Complex Media, 24(4): 357-375 (2014).

[56] R. Nawaz, M. Ayub and A. Javaid, Plane wave diffraction by a fnite plate with impedance boundary conditions , Plos One, 9(4): e92566 (2014).

[57] R. Nawaz, A. Wahab and A. Rasheed, An intermediate range solution to a diffraction problem with impedance conditions, Modern Optics, 61(16): 1324-1332 (2014).

[58] A. Wahab and R. Nawaz, A note on noise source localization, Vibration and Control, 22(7): 1889-1894 (2016).

[59] M. H. Tiwana, Rab Nawaz, A. B. Mann, Radiation of sound in a semi infinite hard duct inserted axially into a larger infinite lined duct , Analysis and Mathematical Physics, 016-0154-4, s13324 (2017).

[60] M. U. Hassan, M. Naz and R. Nawaz, Reflected Field Analysis of Soft-Hard1 Pentafurcated Waveguide, Advances in Mechanical Engineering, 9(2): 1687814017692697 (2017).

[61] R. I. Nuruddeen, R. Nawaz and Q. M. Z. Zia, Dispersion of Elastic Waves in an Asymmetric Three-Layered Structure in the Presence of Magnetic and Rotational Effects, Progress In Electromagnet M, 91: 165-177 (2020).

[62] R. I. Nuruddeen, R. Nawaz and Q. M. Z. Zia, Asymptotic analysis of an anti-plane shear dispersion of an elastic five-layered structure amidst contrasting properties, Arch Appl Mech, 90: 1875-1892 (2020).

[63] R. I. Nuruddeen, R. Nawaz and Q. M. Z. Zia, Investigating the viscous damping effects on the propagation of Rayleigh waves in a three-layered inhomogeneous plate, Physica Scripta, 95(065224): 1-11 (2020).

[64] R. I. Nuruddeen, R. Nawaz and Q. M. Z. Zia, Effects of thermal stress, magnetic field and rotation on the dispersion of elastic waves in an inhomogeneous five- layered plate with alternating components, Science Progress, 103(3): 1-22 (2020).

[65] R. I. Nuruddeen, R. Nawaz and Q. M. Z. Zia, An asymptotic investigation of the dynamics and dispersion of an elastic five-layered plate for anti-plane shear vibration, Journal of Engineering Mathematics, 128(1): 1-12 (2021).

[66] R. I. Nuruddeen, R. Nawaz and Q. M. Z. Zia, Asymptotic approach to antiplane dynamic problem of asymmetric three-layered composite plate, Mathematical Methods in the Applied Sciences, 44(14): 10933-10947 (2021).

[67] L. E. Kinsler, A. R, Frey, A. B. Coppens and J. V. Sanders, Hand book, Fundamental of accoustics, 4th Edition, Wiley (1999).

[68] R. Kirby and A. Cummings, Prediction of the bulk Acoustic properties of fibrous materials at low frequencies, Applied Acoustics, 56(2): 101-125 (1999).

[69] M. Afzal, R. Nawaz, M. Ayub, and A. Wahab, Acoustic scattering in flexible waveguide involving step discontinuity, PloS one, 9(8): e103807 (2014).

[70] A. Cummings, Low frequency acoustic transmission through the walls of rectangular ducts, Journal of Sound and Vibration, 61(3): 327-345 (1978).

[71] A. Cummings, Stiffness control of low frequency acoustic transmission through the walls of rectangular ducts, Journal of Sound and Vibration, 74(3): 351-380 (1981).

[72] P. M. Morse, The transmission of sound inside pipes, The Journal of the Acoustical Society of America, 11(2): 205-210(1939).

[73] R. Kirby, A. Cummings, Prediction of the bulk Acoustic properties of brous materials at low frequencies, Applied acoustics, 56: 101-125(1999) .